An ensemble-based assessment of bias adjustment performance, changes in hydrometeorological predictors and compound extreme events in EAS-CORDEX

Patrick Olschewski, Patrick Laux, Jianhui Wei, Brian Böker, Zhan Tian, Laixiang Sun, Harald Kunstmann

Angaben zur Veröffentlichung / Publication details:

Olschewski, Patrick, Patrick Laux, Jianhui Wei, Brian Böker, Zhan Tian, Laixiang Sun, and Harald Kunstmann. 2023. "An ensemble-based assessment of bias adjustment performance, changes in hydrometeorological predictors and compound extreme events in EAS-CORDEX." *Weather and Climate Extremes* 39: 100531. https://doi.org/10.1016/j.wace.2022.100531.

Weather and Climate Extremes 39 (2023) 100531

Contents lists available at ScienceDirect

Weather and Climate Extremes

journal homepage: www.elsevier.com/locate/wace

An ensemble-based assessment of bias adjustment performance, changes in hydrometeorological predictors and compound extreme events in EAS-CORDEX

Patrick Olschewski [a,*], Patrick Laux [a,b], Jianhui Wei [a], Brian Böker [a], Zhan Tian [c,d], Laixiang Sun [e,f], Harald Kunstmann [a,b]

[a] Karlsruhe Institute of Technology - Campus Alpin, Garmisch-Partenkirchen, Germany
[b] University of Augsburg - Institute of Geography, Augsburg, Germany
[c] School of Environmental Science and Engineering, Southern University of Science and Technology, Shenzhen, China
[d] Pengcheng Laboratory, Shenzhen, China
[e] Department of Geographical Sciences, University of Maryland, College Park, MD, USA
[f] School of Finance & Management, SOAS University of London, London, UK

ARTICLE INFO

Dataset link: https://cds.climate.copernicus.eu/cdsapp#!/dataset/reanalysis-era5-pressure-levels?tab=overview, https://esgf-data.dkrz.de/search/esgf-dkrz/

Keywords:
Model evaluation
Bias adjustment
Uncertainty assessment
Predictions
Compound events
East asia

ABSTRACT

The effectiveness of adaptive measures tackling the effects of climate change is dependent on robust climate projections. This becomes even more important in the face of intensifying extreme events. One example of these events is flooding, which embodies a major threat to highly vulnerable coastal urban areas. This includes eastern Asia, where multiple coastal megacities are located, e.g. Shanghai and Shenzhen. While the ability of general circulation models (GCMs) and regional climate models (RCMs) to project atmospheric changes associated with these events has improved, systematic errors (biases) remain. This study therefore assess capabilities of improving the quality of regional climate projections for eastern Asia. This is performed by evaluating an ensemble consisting of bias adjustment methods, GCM-RCM model runs and future emission scenarios based on representative concentration pathways (RCP) obtained from EAS-CORDEX. We show that bias adjustment significantly improves the quality of model output and best results are obtained by applying quantile delta mapping. Based on these results we evaluate potential future changes in crucial hydrometeorological predictors, univariate extreme events and compound extreme events, focusing on high wind speeds and extreme precipitation. Key findings include an increase in daily maximum temperature of 1.5 to nearly 4 °C, depending on the scenario, as well as increased levels of precipitation under RCP 8.5. Furthermore, a distinct intensification of extreme events including high temperatures and heavy precipitation is detected and this increase exceeds the increase of the overall mean of these predictors. The annual number of compound events including heavy precipitation and extreme wind speeds shows a significant increase of up to 50% for RCP 8.5 in the South China Sea as well as the adjacent coastal areas.

1. Introduction

Dynamic atmospheric models have become a valuable source of information, not only for weather predictions, but also in the field of climatology. An increase in computational capacities, a better understanding of the underlying physical processes and a growing fund of experience have led to an improvement in the quality of model output. In this context, the Intergovernmental Panel on Climate Change (IPCC) has elaborated a series of plausible scenarios for the end of the 21st century, bearing important drivers for the environmental system, including levels of greenhouse gases, population statistics and the sustainability of predominant resources (IPCC, 2021). The simulations of these drivers are provided on a global basis and can be used to run global atmospheric or coupled atmospheric-oceanic models (Wilby and Harris, 2006), unveiling global trends in crucial predictors (e.g. temperature, precipitation) and offering projections of future climate change until the end of the 21st century. However, the spatial resolution of GCMs and the representation of specific climate-related characteristics remains unsatisfactory when aiming at precise projections on a local and regional scale.

* Corresponding author.
E-mail address: patrick.olschewski@kit.edu (P. Olschewski).

https://doi.org/10.1016/j.wace.2022.100531
Received 1 August 2022; Received in revised form 19 October 2022; Accepted 24 November 2022
Available online 26 November 2022

Regional refinement, i.e. downscaling, therefore becomes necessary, when aiming at predictions with a higher resolution. Maurer and Hidalgo (2008). While the dynamical approach, one of two main approaches, is performed by nesting a high-resolution regional climate model driven by the output of global models (Giorgi, 2019; Giorgi et al., 2001), the statistical approach is based on statistical relations between the large-scale and local atmospheric state (Hewitson and Crane, 1996; Maraun et al., 2010; Jacobeit et al., 2014). To further improve the quality of the output of these downscaling methods, the statistical method of bias adjustment can be applied by obtaining statistical characteristics in the reference data set and adopting these to the model output by applying a specified transfer function.

In the wake of the development and improvement of these tools, scientific research has established a linkage between climate change and extreme events, potentially leading to an increase in frequency and intensity (IPCC, 2021). While the effects of and potential changes in specific univariate extreme events, e.g. droughts, heat waves, heavy precipitation, have been extensively studied in the past, the scientific focus has recently shifted towards co-occurring extreme events of more than one predictor, i.e. compound events. Zscheischler et al. (2020) offered a classification of different types of compound events, with the "compounding" factor being either based on location, time, variables, or preconditions. The authors also point out the high relevance of compound events under a changing climate, and their statements are complemented by Zhang et al. (2021), who discuss disproportionate socioeconomic effects of compound events when compared to univariate extreme events. Although many types of compound events have proven to be of interest towards further scientific research, e.g. heat and drought, precipitation and streamflow, heat and fire danger, this article focuses on tropical cyclones as a specific representative of compound events including extreme wind speeds and precipitation amounts. Attempts exist towards an overall, global quantification of the projected changes in compound events in general, as well as tropical cyclones in specific, which are in detail discussed in the latest reports of the (IPCC, 2013, 2021). However, a variety of studies addressing this issue demonstrate regional variations from the general trend and the necessity for basin-specific analyses (Messmer and Simmonds, 2021; Torres-Alavez et al., 2021; Knutson et al., 2020; Ridder et al., 2020).

Of the affected areas worldwide, the northwest Pacific stands out in particular. This is mainly due to the high density of coastal cities and megacities, e.g. Shanghai, Shenzhen, Guangzhou, and Manila. Due to their high population density, these urban areas are in particular under threat by floods and typhoons, accompanied by potentially devastating environmental and socioeconomic consequences as well as threats to human life. This is further potentiated by ongoing human-caused influences on the earth system, for example urbanization, sea-level rise and climate change. Taking multiple of these risk factors into account, Balica et al. (2012) demonstrated Shanghai and Manila to be among the most vulnerable cities towards flooding events worldwide. This confirms the findings of Hanson et al. (2011), according to which the majority of cities with the highest population exposure to coastal flooding in the future is located in East and Southeast Asia, including Shanghai, Guangzhou, and Ho Chi Minh City. The risk for coastal cities is even more amplified by impacts of compounding extreme events, as demonstrated by Xu et al. (2022b). Especially in rapidly growing megacities like Shenzhen, impacts of climate change may not only multiply the associated risks (Sarica et al., 2021), but effective adaption strategies could also be implemented within the development process of the city, if reliable projections are available (Ke et al., 2021, 2020).

In this concern, it is the objective of this study to contribute optimized projections of long-term climate change as well as extreme events and compound events in the East Asian domain. In the context of Zscheischler et al. (2020), we consider compound events as events of multiple variables, taking place at the same time and location. While many studies focus on either optimized bias adjustment or potential changes in hydrometeorological parameters under climate change, this research aims at comprehensively combining both aspects of climatology. This article therefore seeks contribute to the following questions: (a) Does the application of statistical bias adjustment affect the data quality of model output and what methods are suitable? (b) How does long-term projected climate change under different scenarios manifest itself in the study domain for crucial hydrometeorological predictors? (c) What changes in univariate extreme events and compound events including extreme wind speeds and heavy precipitation are expected under climate change scenarios and what regions will be affected by these changes?

The article is structured as follows: Section 2 introduces the applied data sets and statistical methods. The latter include bias adjustment methods, tools for model evaluation, performance measures and thresholds of extreme events. Results are presented in Section 3 and structured according to the given research questions into bias adjustment, long-term atmospheric changes and extreme events. The results are subsequently discussed in Section 4 and concluding remarks are given in Section 5.

2. Data and methods

2.1. Data

The acquired data sets for this study can be distinguished into (a) model runs of a specific scenario for a future period, (b) historical model runs for each of the selected future model setups spanning an observed time period, and (c) reanalysis data spanning the same observed time period for validation purposes. The former originate from the **CO**ordinated **R**egional Climate **D**ownscaling **EX**periment (CORDEX), providing dynamically downscaled data sets using global and regional circulation models. The latter is obtained from the latest-generation ERA5 reanalysis of the European Centre for Medium-Range Weather Forecasts (ECMWF). All utilized data sets are displayed in Table 1 and are described in detail below. Included variables are 2 m maximum temperature, daily accumulated precipitation, 10 m maximum wind speed, and surface pressure. All variables, corresponding base units and units of changes, as well as climate indices and definitions utilized in this study are given in Table 2.

2.1.1. CORDEX model output

One contributor of dynamically downscaled climate data is CORDEX, a Model Intercomparison Project initiated by the World Climate Research Programme WCRP (Giorgi et al., 2009). For our analysis, downscaled CORDEX model data is retrieved for the East Asian domain "EAS" (CORDEX, 2022). Of two available resolutions (0.22° × 0.22° and 0.44° × 0.44° on a rotated grid), historical model runs as well as the two existing future runs of all GCM-RCM combinations for the Representative Concentration Pathways (RCP) 2.6 and 8.5 are acquired for the finer resolution. For the recently published Shared Socioeconomic Pathways (SSP), which are similar but not equatable regarding the former RCP scenarios (IPCC, 2021), downscaled model output was not yet sufficiently provided for this analysis. For our domain, available GCM output includes the models MOHC-HadGEM2-ES (Collins et al., 2011), MPI-ESM (Jungclaus et al., 2013; Stevens et al., 2013) and NCC-NorESM1-M (Bentsen et al., 2013; Iversen et al., 2013). RCMs include REMO2015 (Jacob et al., 2012; Jacob, 2001) and RegCM4-4 (Giorgi et al., 2012). We therefore consider six GCM-RCM combinations. CORDEX also provides a set of RCM simulations driven by reanalysis data (Tang et al., 2022). While these simulations offer further insights into the structure of inherited bias, it is the aim of this study to specifically assess the joint bias arising from the combination of the specific GCMs and RCMs, which is why the historical experiments were obtained. An additional assessment of the bias inherited only in the RCMs, which can be conducted using reanalysis-driven runs, was beyond the scope of this analysis.

Table 1
Datasets utilized in this study. First column depicts term used for the corresponding GCM-RCM combination. For CORDEX, underlying GCMs and RCMs are given, as well as the provided time span for the historic, RCP 2.6 and RCP 8.5 model runs. ERA5 is reanalysis data set obtained from ECMWF used for reference purposes.

Name in present study	GCM	RCM	Historical	RCP 2.6	RCP 8.5
HadGEM2-RegCM4-4	MOHC-HadGEM2-ES	RegCM4-4	1970–2005	2006–2098	2006–2099
HadGEM2-REMO2015	MOHC-HadGEM2-ES	REMO2015	1970–2005	2006–2099	2006–2099
MPI-ESM-RegCM4-4	MPI-ESM-MR	RegCM4-4	1980–2005	2006–2099	2006–2099
MPI-ESM-REMO2015	MPI-ESM-LR	REMO2015	1970–2005	2006–2100	2006–2100
NorESM1-RegCM4-4	NCC-NorESM1-M	RegCM4-4	1970–2005	2006–2099	2006–2100
NorESM1-REMO2015	NCC-NorESM1-M	REMO2015	1970–2005	2006–2100	2006–2100
ERA5	–	–	1979–present	–	–

Table 2
Variables and definitions of extreme events and climate indices used in this study and corresponding base units and units of changes.

Variable	Base unit	Changes in variable (Δ)
Daily maximum 2 m air temperature	°C	°C
Daily accumulated precipitation	mm	%
Daily maximum 10 m wind speed	m s^{-1}	m s^{-1}
Daily mean surface pressure	hPa	hPa
Definitions of extreme events	**Daily max. wind speed**	**Daily precipitation**
Tropical cyclone-force wind event (Walsh et al., 2007)	>17.5 m s^{-1}	–
Compound event	>17.5 m s^{-1}	>99th percentile
Definitions of climate indices	**Base unit**	**Changes in index (Δ)**
Annual number of days with tropical cyclone-force winds	d	d a^{-1}
Annual number of days with compound events	d	d a^{-1}

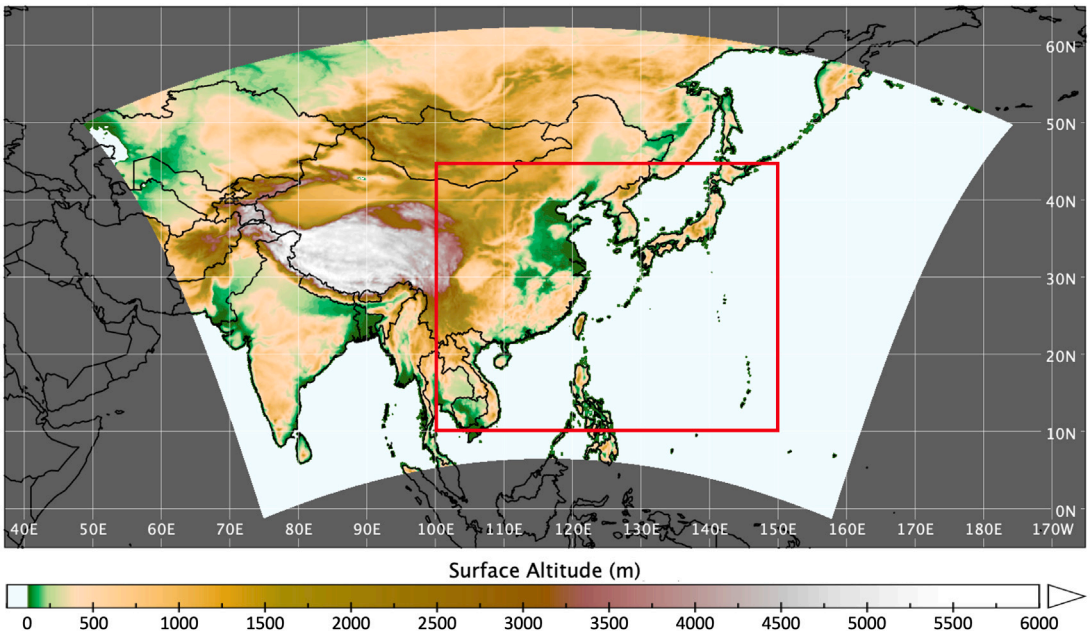

Fig. 1. Domain in present study. EAS-CORDEX outer domain in colours, analysed area enclosed in red. (For interpretation of the references to colour in this figure legend, the reader is referred to the web version of this article.)

To match the structure of the validation data, all data sets were bilinearly interpolated onto a 0.25° × 0.25° regular grid, following similar analyses of, for example, Chakraborty et al. (2021) and Shen et al. (2020). The suitability of bilinear interpolation regarding precipitation data in EAS-CORDEX was also demonstrated by Feng et al. (2019). To account for the model with the shortest temporal availability, the validation is performed for the period 1981–2005 and future runs are analysed for the periods 2040–2059 (mid-future) and 2080–2099 (distant future). Further, as the HadGEM2-RegCM4-4 model combination does not span the entire future period for the RCP scenario 2.6, ending in the year 2098, analyses for the distant future for this specific model include the year 2079.

2.1.2. ERA5 reanalysis

To overcome limited data availability in regions with a low density of measuring stations, several other data sources can be consulted. For example, observation data from multiple sources and data sets can be assimilated and interpolated to obtain equally distributed spatial data (Van Den Besselaar et al., 2017). Also, station-based data can be combined with satellite-based data, e.g. in remote locations without a sufficient accessibility (Lahoz and Schneider, 2014; Carrassi et al., 2018; Cornes et al., 2018). Another approach is the performance of reanalysis, in which an atmospheric model is driven by assimilated observations (Wong et al., 2017). This bears the advantage of *physical coherence*, as stated by Dee et al. (2011), abiding the laws of physics

in an intrinsic, spatially consistent model, yet maintaining the characteristics of the underlying observations. This type of reference data is suitable for our analysis, offering precise data for densely populated regions, yet also providing spatially consistent data for remote locations, i.e. over the Pacific Ocean. It also simplifies a spatial comparison with the similarly structured future model runs. Many well-established reanalysis products exist, e.g. by JMA (Shinya et al., 2015; Harada et al., 2016), ECMWF (Hersbach and Dee, 2016; Hersbach et al., 2020), and NCAR (Kalnay et al., 1996; Kanamitsu et al., 2002). As it fits best to our selected future models runs in terms of spatial and temporal availability, daily ERA5 reanalysis data (Hersbach et al., 2018) for the greater East Asian domain 100°−150° E, 10°−45°N (see Fig. 1) on a regular grid was obtained as a reference for validation. The data set for each variable has a resolution of 0.25° × 0.25° and was retrieved for the period 1981–2020. Since wind speed is not directly available from the data store, u (west to east velocity) and v (south to north velocity) vector components were obtained separately and accordingly assembled.

2.2. Methods

The main methodological focus of this analysis was the assessment of uncertainties in the output of the downscaled model data and the optimization of this output by applying a variety of bias adjustment methods. The performance of these methods was evaluated by applying a cross validation procedure and interpreting the results using Taylor diagrams as well as statistics regarding climatology. This section is concluded by highlighting the applied performance measures and the utilized thresholds for the detection of extreme events. Note, that bias adjustment for the time series of each grid cell is performed first and extreme events are subsequently derived using the adjusted data sets.

2.2.1. Bias adjustment methods

As stated above, an improvement in the quality of local climate projections can be achieved by performing downscaling. However, a variety of sources for bias remains. This includes, for example, systematic bias in the GCMs, the inability of *free-running* models to correctly render the daily variability as well as physical simplifications in the model setup. These three sources of bias are classified and in detail described by Eden et al. (2012). It is therefore of high importance for the effectiveness of protective measures and adaptive strategies to quantify uncertainties in model output as well as to debias. This leads to the first objective of this study, to address and correct uncertainties in the output of GCM-driven regional climate models. As stated by Gudmundsson et al. (2012), it is in this context necessary to (a) compare the performance of different bias adjustment methods, and (b) find an appropriate solution towards the application of bias adjustment methods to the raw model output.

A variety of approaches towards the correction of biases exists, of which many have proven to be suitable and effective towards their intended application. In a simplistic approach, a correction of output data can be achieved by applying the "delta method", i.e. by adding or multiplying a constant, accounting especially for systematic errors (Deque, 2007). A different approach is the application of quantile mapping methods. In general, this describes a statistical transformation that is performed on the intensity distribution function of the raw data to fit the corresponding intensity distribution function of the reference data (Piani et al., 2010b) and is expressed as:

$$x_{bc} = f(x_{m,p}), \tag{1}$$

with x_{bc} denoting the adjusted sample, f the transformation function and $x_{m,p}$ the raw data.

Several approaches to find f exist and are in detail discussed by Gudmundsson et al. (2012). These include, for example, parametric functions, for which the quantile–quantile relation of model and reference data is fitted using adjustable parameters. x_{bc} is then estimated using, for example, scale-based adjustments, as in $\hat{x}_{bc} = b\ x_{m,p}$, or linear adjustments, as in $\hat{x}_{bc} = a + b\ x_{m,p}$. Under the assumption of an underlying theoretical distribution, the distribution function can be adjusted, if the parameters necessary to fit the theoretical distribution are appropriately estimated. The choice of an adequate distribution is dependent on the variable, e.g. Li et al. (2019) and Haas et al. (2014) prove the Weibull distribution to be a suitable choice for the correction of wind speed. Shin et al. (2019), Piani et al. (2010a), and Ines and Hansen (2006) demonstrate the Gamma function to be suitable for application to precipitation data, and Teutschbein and Seibert (2012) the Gaussian distribution for temperature. The quantile–quantile relation can also be non-parametrically adjusted using spline functions (Kouhestani et al., 2016). Regarding the nature of the spline function, Gudmundsson et al. (2012) recommend the use of cubic smoothing splines. Another approach is to correct the density function of the sample according to the corresponding density function of the reference data based of the underlying percentiles. Based on Boé et al. (2007), this method is referred to as "empirical quantile mapping" and performs a percentile-wise empirical estimation and corrects bias according to differences in the percentile estimations as well as linear interpolation for values within two percentiles. As for smoothing spline adjustment, this is also a non-parametric approach, because percentile-wise correction is solely dependent on the structure of the reference data and therefore does not require an assumed underlying theoretical distribution (Themeßl et al., 2012). Using these methods and provided the cumulative distribution function (CDF) F is given, x_{bc} can also be obtained by applying

$$F_{m,c}(x_{m,c}) = F_{o,c}(x_{o,c}) \tag{2}$$

and

$$x_{bc} = F_{o,c}^{-1}[F_{m,p}(x_{m,p})], \tag{3}$$

where $F_{o,c}$ is the CDF of the reference sample and $F_{m,p}$ the CDF of the uncorrected data (Tong et al., 2021). As the authors show, this two-step correction is necessary when correcting independent time series, i.e. future time series or validation periods. First, the necessary correction for the model data in an observed time period must be obtained by applying Eq. (2). For the variable of interest x within the observed period ($_c$), the CDF of the model data ($F_{m,c}$) is first fitted to the CDF of the reference data ($F_{o,c}$). This adjusted series can then be subject to validation. Next, under the assumption that the bias structure is time-independent for the observed and future period, the transformation function obtained from the observed model series is applied to the future series. As given in Eq. (3), the CDF of the model data in the projected period ($F_{m,p}$) is fitted to $F_{o,c}$ to obtain the bias adjusted sample x_{bc}. Note, that the inverse of $F_{o,c}$ is applied.

It becomes apparent from Eqs. (2) and (3), that model values exceeding (undercutting) the CDF range of the reference data will be adjusted to match the CDF of the reference data, resulting in a disturbance of extremes and potential future changes. To account for this, Boé et al. (2007) and Themeßl et al. (2012) suggest the correction of *"new extremes"* according to the correction that is performed for the highest (lowest) percentile of the reference period, which is also applied in this study. Furthermore, demonstrated by Maurer and Pierce (2014) and Maraun (2013), empirical quantile mapping may lead to an unintentional perturbation of trends in the model, resulting in an additional source of bias.

Whether original trends in the model output should be preserved is also discussed by Cannon et al. (2015) and the method of quantile delta mapping is introduced. Accordingly, the relative linear trend Δ_m for a specific time step t is defined as

$$\Delta_m(t) = \frac{x_{m,p}(t)}{F_{m,c}^{-1}[F_{m,p}^{t}[x_{m,p}(t)]]}. \tag{4}$$

Subsequently, the adjusted value for the corresponding time step $\hat{x}_{bc}(t)$ is modified by applying

$$\hat{x}_{bc,\Delta}(t) = \hat{x}_{bc}(t)\Delta_m(t) \tag{5}$$

to form the quantile delta adjusted value $\hat{x}_{bc,\Delta}(t)$. Therefore, the original trend in the model is preserved. As the authors show, this approach also allows for an additive preservation of trends, by applying

$$\Delta_m(t) = x_{m,p}(t) - F^{-1}_{m,c}[F^t_{m,p}[x_{m,p}(t)]], \tag{6}$$

and

$$\hat{x}_{bc,\Delta}(t) = \hat{x}_{bc}(t) + \Delta_m(t), \tag{7}$$

subsequently.

For all consulted methods an adjustment for the number of precipitation days was performed. According to Piani et al. (2010b) this can be achieved by applying a transfer of the number of wet days in the reference period to the model data. This is necessary, as models tend to overestimate the number of wet days due to drizzle-effects (Maraun, 2016; Piani et al., 2010b; Gutowski et al., 2003). Starting from the day with the least precipitation amount, days with non-zero values are set to 0 until the wet day threshold obtained from the reference data is reached. As a constraint and following (Gudmundsson et al., 2012), daily precipitation sums exceeding 0.1 mm d^{-1} are upheld.

A plurality of studies aiming for the single method with the best performance exists. However, as (Laux et al., 2021) point out, an improvement in the uncertainty assessment can be achieved by constructing an ensemble of multiple bias adjustment methods, as bias adjustment itself can possibly even increase the bias in the post-processed data. We therefore assessed the most promising bias adjustment techniques, based on literature review and statistical evaluation, and quantified the benefits regarding single-method-based and ensemble-based approaches. Preliminary literature review reveals an unequivocal picture of the suitability of the bias adjustment methods presented above. While authors point out that most methods are capable of reducing bias in raw model output, a majority of studies relies on empirical quantile mapping and quantile delta mapping as they perform most effective with regard to the respective evaluation criteria (Tong et al., 2021; Laux et al., 2021; Shen et al., 2020; Enayati et al., 2021; Heo et al., 2019; Choudhary and Dimri, 2019). According to Gudmundsson et al. (2012), smoothing spline-based bias adjustment is also a promising approach and can generate a similar improvement. As the non-parametric approaches outperform those implying a theoretical distribution, and this can be seen for multiple atmospheric variables, we proceeded close to the approach of Kouhestani et al. (2016), including three non-parametric approaches in the detailed analysis, i.e. smoothing spline-based bias adjustment (SSPLIN), empirical quantile mapping (QUANT) and quantile delta mapping (QDM).

The bias adjustment and evaluation procedure allows for the evaluation of (a) differences in the performance of each investigated bias adjustment method, (b) the uncertainties within the 30 cross validated ensemble members of a specific model setup, and (c) the overall performance of a specific bias adjustment method for the single models and ensemble mean. Regarding (a) and (b) Taylor diagrams have proven suitable for a concise evaluation of bias adjustment performance, as well as differences within models and correction methods.

2.2.2. Evaluation of methods and models

To evaluate the performance of a specific bias adjustment method, the transformation function computed for the reference period, i.e. the calibration period, can be applied to a second, independent period, i.e. the validation period, that is not included in calibration. This approach follows the assumption that the bias structure is stationary, i.e. no change in bias for future periods occurs and effective corrections for reference periods equally apply to independent periods (Cannon et al., 2015; Maraun, 2012; Maraun et al., 2010). Nevertheless, regarding potential time-dependencies in the model bias, further research suggests that validation using a single time period may not be sufficient to provide robust results (Miao et al., 2016; Li et al., 2010; Reifen and Toumi, 2009). We therefore applied a cross validation procedure that is introduced by Miao et al. (2016) and similarly used by Shen et al. (2020) to each GCM-RCM combination and each bias adjustment method. Out of the years 1981–2005, 20 years were chosen on a random basis and used for calibration. The remaining five years that are not included in the calibration period are unknown to the transformation function and hence used as independent validation period. This procedure was repeated 30 times, for each of which a new set of five validation years out of the period 1981–2005 was randomly assigned, and the remaining 20 years were used for calibration. The random nature of the assignment of the five years for validation guarantees that every year out of 1981–2005 has the same probability of being chosen for validation and the entire period is considered within every of the 30 ensemble members, ensuring the robustness of the performance evaluation. Since no presumption regarding the validity of specific years used for validation can be made, the ensemble mean for each GCM-RCM combination and each bias adjustment method was computed using the equally weighted 30 ensemble members.

To provide further insights into the robustness of our findings, a hypothesis test was applied to gain information on the statistical significance of the projected changes between the future period and the reference period. For each grid cell, the daily series of the reference period was tested against the time series of a future period under the null hypothesis that both samples are equally distributed (Wilcoxon, 1945). Vice versa, if the null hypothesis is rejected for a predefined level of significance, it can be assumed that the distributions differ significantly. For our analysis we define the commonly applied error probability of $\alpha = 0.05$ to indicate statistical significance. As a generalized assumption of Gaussian distribution could not be upheld for all samples, a Mann–Whitney U test was performed (Mann and Whitney, 1947; Student, 1908).

2.2.3. Performance measures

The computation of skill scores opens the opportunity of a simple comparison of two or more entities. A wide range of possibilities exist for the evaluation of model output as, for example, presented by Kotlarski et al. (2014). As the results of this study are mainly reliant on optimized projections of the overall mean and percentile-based thresholds, these metrics are accounted for throughout the evaluation process. Specifically, the overall mean bias, expressed as BIAS, is calculated according to Eq. (8), and the calculation of the mean absolute error (MAE) is shown in Eq. (9). Deviations in percentile-based thresholds are expressed by $\Delta P_n = P_{n,v} - P_{n,o}$, where n is the value of the percentile that is described, e.g. 95 for the 95th percentile, v is the model data that is to be evaluated and o is the reference value. In addition, Taylor diagrams were consulted as they are widely common throughout the field of model evaluation and embody a convenient approach to the evaluation of multiple performance measures (Taylor, 2001; Enayati et al., 2021; Jolliff et al., 2009). These include centralized root mean square error (RMSE, Eq. (10)), correlation coefficient (R, Eq. (11)), and normalized standard deviation (σ_*, Eq. (12)). Within the given equations, t indicates the time step, x_o denotes the reference sample obtained from ERA5, and x_v denotes the bias adjusted sample. All included metrics are calculated for the time series of each of the inspected grid cells by means of Eqs. (8) through (12). Subsequently, the mean of the grid cell-wise results is computed for the study domain and displayed in the corresponding figures.

$$BIAS = \frac{1}{N}\sum_{t=1}^{N}(x_{v,t} - x_{o,t}) \tag{8}$$

$$MAE = \frac{1}{N}\sum_{t=1}^{N}(|x_{v,t} - x_{o,t}|) \tag{9}$$

$$RMSE = \sqrt{\frac{1}{N}\sum_{t=1}^{N}(x_{v,t} - x_{o,t})^2} \tag{10}$$

$$R = \frac{\frac{1}{N}\sum_{t=1}^{N}(x_{o,t} - \overline{x}_o)(x_{v,t} - \overline{x}_v)}{\sigma_o \sigma_v} \tag{11}$$

$$\sigma_* = \frac{\sigma_v}{\sigma_o} \tag{12}$$

A simple approach, BIAS represents the overall mean deviation of the bias adjusted sample x_v and the corresponding reference x_o. It inherits the unit of the analysed variable and is equal to 0 if the two samples are identical. However, this is also the case for a change in the bias structure, e.g. differing magnitudes, without a change in the mean. Therefore MAE and RMSE are considered. While these measures are similar, for example in counteracting the effect of positive and negative bias cancelling each other by considering absolute and squared errors, RMSE places a greater focus on larger deviations. This is due to the forming of squares prior to the summation and conditions the relationship: MAE ≤ RMSE. It is shown by Chai and Draxler (2014) that both metrics, despite their similarity, must be handled individually and can be an equal part of a comprehensive analysis. The authors also point out the robustness of large sample sizes when aiming at the "true" values of RMSE and MAE, beginning at sample sizes of 100 and 5 ensemble members. This is also given for our validation approach that considers sample sizes of ~7300, i.e. 20 years of daily data, and 30 ensemble members.

The correlation coefficient R is a widely used measure to indicate a linkage in the appearance of two samples. If both samples exhibit a similar behaviour for regions of high or low values, this is considered a positive correlation and the coefficient converges towards its upper limit value 1. In the opposite case, i.e. negative correlation, the coefficient value converges to its lower limit −1. For $R = 0$ no correlation can be assumed.

The normalized standard deviation σ_* considers the relation between the standard deviation of the bias adjusted sample and the reference. If the standard deviations in both samples are equal, σ_* reaches 1.

2.2.4. Definition of extreme events

The adequate choice of threshold for the definition of extreme events has for a long time been subject of scientific discourse (Zhang et al., 2011). This analysis focuses on percentile-based thresholds, which are also issued by the Expert Team on Climate Change Detection and Indices (ETCCDI, 2022). As the obtained data sets comprise daily data, an extreme event referring to the 99th percentile, for example, statistically occurs once every 100 days, or three to four times in one year, respectively. To account for varying definitions and suggestions in the literature regarding the optimum percentile to be used as threshold (Zhang et al., 2011; Guzzetti et al., 2008), the analysis of univariate extreme events is based on thresholds ranging from the first to the 99th percentile.

To what extent tropical cyclones, within our study region referred to as typhoons, are adequately represented in reanalysis and climate models has been subject to intensive research (Jin et al., 2016; Truchelut et al., 2013; Truchelut and Hart, 2011; Emanuel, 2010; Bengtsson et al., 2007; Walsh, 1997). A common source of uncertainty within these analyses is the under-representation of extreme events, e.g. typhoons, due to the broad underlying grid cell structure. To account for this issue we followed the approach of Walsh et al. (2007) and adopted the proposed threshold for tropical cyclone-force winds of 17.5 m s^{-1} at 10 m for a grid resolution of 0.25°. We also adopted the authors' approach to limit potential influences of extratropical wind events by limiting the analysis of days with tropical cyclone-force winds to regions south of 30°N.

As a compound extreme event is defined as an extreme event of two or more variables, we extended the analysis of tropical cyclone-force winds by adding the constraint of daily precipitation above the 99th percentile, relating to "extremely wet days" (ETCCDI, 2022). In accordance with Martius et al. (2016) we allowed for a time separation of one day, to account for events taking place beyond midnight and events with an immediate relation. The latter, for example, allows for the inclusion of storm events on one day, followed by an extreme precipitation event on the next day, into the count of compound events.

3. Results

3.1. Bias adjustment

For maximum air temperature results show an overall good agreement of the raw model output and reanalysis data (Fig. 2). Across all models, notable improvements in data quality appear primarily for the simulated standard deviation, while correlation is sustained at 0.75–0.8 and RMSE is slightly reduced to ~0.7. Regarding precipitation, notable differences in the raw model output become apparent, as deviations based on GCM-RCM combinations including RegCM4-4 are generally lower. Across all models, corrections lead to an alignment in the data quality and an improvement in the normalized standard deviation, however correlation remains low and a notable RMSE remains. This also applies to maximum wind speed and surface pressure. For the former, the picture in the quality of raw data is reversed, as models based on REMO2015 show a higher consistency. For the latter consistency in the quality of the raw model output is higher. The similar performance of QUANT and QDM becomes apparent across all variables, whereas SSPLIN falls short for precipitation and surface pressure. While the overall data structure, expressed by the standard deviation, is notably improved, bias regarding daily variability remains. Due to the similarity in the results of QUANT and QDM we show only the Taylor diagram for the 30 cross validated ensemble members of the latter in Appendix A. The ensemble spread is similar across all variables and no noteworthy outliers appear, indicating the robustness in the chosen reference period.

To further investigate the long-term robustness of the adjusted data we evaluated BIAS and MAE for the raw data as well as SSPLIN, QUANT, and QDM (Fig. 3). Shown are the performance metrics of the model mean, consisting of 30 cross validated ensemble members. It becomes clear that the raw model output inherits significant bias. Moreover, for most models and across all variables positive BIAS is more frequent than negative BIAS. While for maximum temperature and depending on the model setup, the mean deviation reaches up to +1 °C, for precipitation up to +1.7 mm, +3 m s^{-1} for maximum wind speed, and +3.6 hPa for surface pressure, BIAS is reduced to nearly zero after applying QUANT and QDM. For SSPLIN minimal BIAS remains. An exception is maximum wind speed, for which all correction methods reduce BIAS to zero.

Across all variables, a reduction in MAE can also be achieved, however a residue remains. For maximum wind speed and surface pressure, reductions in MAE are the strongest, with reductions of up to 50%. This accounts for up to ~2 m s^{-1} for wind speed and ~4 hPa for surface pressure. For maximum temperature and precipitation MAE reduction is less pronounced, resulting in reductions of up to 0.5 °C and 2 mm, respectively.

The analysis of the correction of percentile thresholds shows a similar picture, as shown for the 95th and 99th percentile (Fig. 4). All bias adjustment methods are capable of reducing deviations of downscaled percentiles from reanalysis-based percentiles. Smoothing spline correction embodies an exception to this in the case of surface pressure, leading even to an increase in percentile deviations. For an analysis of this anomaly please refer to the discussion section. Corresponding to BIAS and MAE, a majority of raw models inherits a positive deviation resulting from an overestimation of the regarded variables. After the performance of bias adjustment, the error margins are notably reduced. For maximum daily temperature and regarding the domain mean, the deviation of both thresholds lies within a margin of ±0.25 °C. For precipitation error margins for the 95th percentile are smaller (±0.5 mm) than for the 99th percentile (±1.5 mm). In the case of maximum wind speed the correction of the in general overestimated percentile thresholds led to a slight overcorrection for all included models. The resulting errors lie within a range from −0.1 to −0.3 m s^{-1} (95th percentile) and −0.3 to −0.7 m s^{-1} (99th percentile). While smoothing spline-based correction leads to an increased overestimation

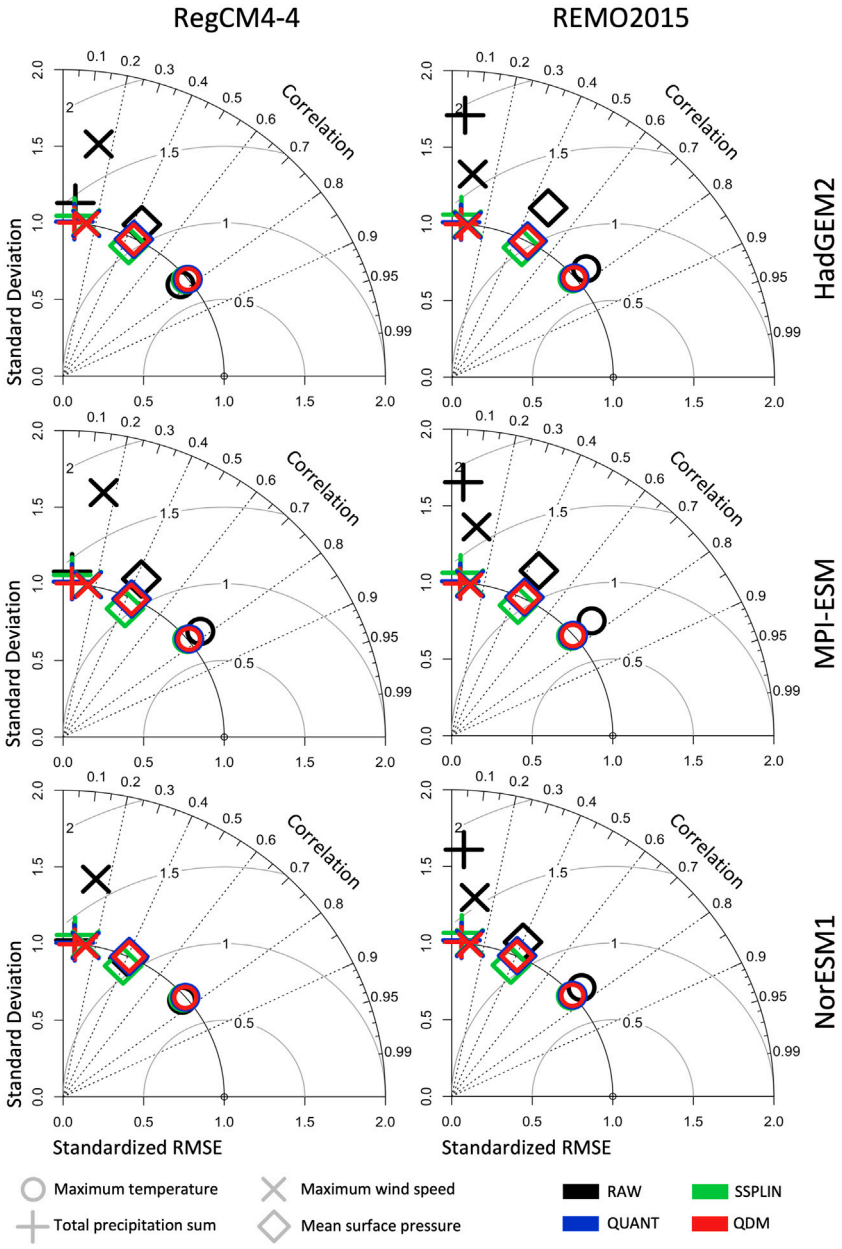

Fig. 2. Taylor diagrams to evaluate the performance of three bias adjustment methods. The underlying GCM and RCM of each of the six model combinations is given in the row label and column label, respectively. The four variables are distinguished by symbols, the bias adjustment methods by colours. Taylor diagrams consist of correlation, normalized RMSE and normalized standard deviation. (For interpretation of the references to colour in this figure legend, the reader is referred to the web version of this article.)

of daily mean surface pressure by up to +5 hPa, depending on the selected model, the error margin for QUANT and QDM spans the range from −0.1 to +0.4 hPa over both percentile thresholds. Across all predictors we regard the results of QUANT and QDM as acceptable for a percentile-based analysis of the climate change signal and based on the preceeding analysis and the statistical advantages, we proceeded with the detailed analysis of the chosen predictors using the bias adjusted data based on QDM.

3.2. Long-term climate change

Regarding climatological changes in the study region, we analysed the long-term annual changes in the bias adjusted annual model data, as well as changes within the spectrum of percentiles for the daily data. While the former provides an overview of the overall expected change for a specific predictor, the latter provides information on changes in the structure of the predictor. For example, an increase in the lower and upper percentiles indicates an increase in the frequency of daily extremes, setting the link to the subsequent analysis comprising of percentile-based extreme events and predefined thresholds of compound events.

3.2.1. Maximum temperature

Long-term climatological change (Fig. 5 (a), left) shows a steady increase in the annual mean of the daily maximum temperature for the RCP 8.5 scenario, leading to maximum temperatures 3.8 °C higher in

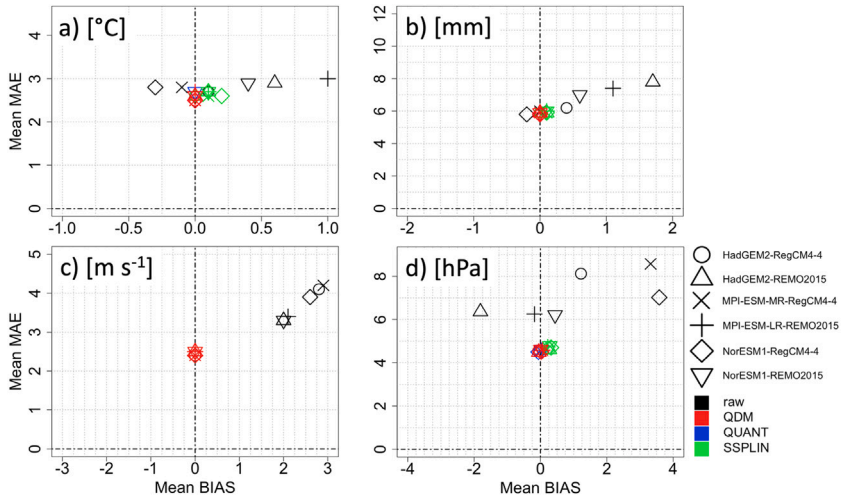

Fig. 3. Evaluation of BIAS and MAE within the validation period 1981–2005 for three non-parametric bias adjustment methods (black: raw, green: SSPLIN, blue: QUANT, red: QDM). (a) daily maximum air temperature, (b) daily precipitation sum, (c) daily maximum wind speed, (d) daily mean surface pressure. (For interpretation of the references to colour in this figure legend, the reader is referred to the web version of this article.)

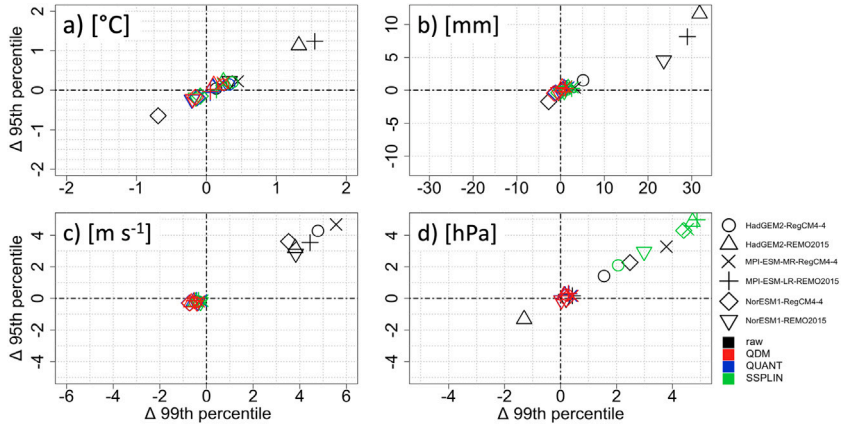

Fig. 4. Evaluation of accuracy in the representation of percentiles for three non-parametric bias adjustment methods (black — raw, green — SSPLIN, blue — QUANT, red — QDM). (a) daily maximum air temperature, (b) daily precipitation sum, (c) daily maximum wind speed, (d) daily mean surface pressure. (For interpretation of the references to colour in this figure legend, the reader is referred to the web version of this article.)

2080–2099 when referring to 1981–2000. The deviation of the single models from this trend is ±1 °C. Under scenario RCP 2.6, temperatures are to increase until the middle of the 21st century and reach a mean increase of 1.5 °C, then tending to a slight decrease until the end of the century. Changes in percentiles (Fig. 5 (a), right) indicate a stronger contribution of daily extremes to the overall change. The increase for days below the 30th and above the 95th percentile exceeds the corresponding mean increase across all scenarios and time periods. While changes remain mostly within a threshold of + 1.5 °C for RCP 2.6, extremes exceed the overall mean change by up to 1 °C for scenario RCP 8.5, e.g. leading to temperatures 4.5 °C higher on hot days with a return period of 100 days until the end of the century.

In terms of the spatial distribution, two gradients become apparent (Fig. 6). On the one hand side, warming is predicted to be more intense over continental masses than over the Pacific, on the other hand warming increases with northward latitude. For the RCP 2.6 scenario maximum temperature increases by up to 2 °C for most regions above 30° *N* and continental masses further south. Maximum temperatures are increased by up to 1 °C over maritime regions south of 30° N, aggregating to the described overall mean change of +1 to +1.5 °C. For the RCP 8.5 scenario spatial structures remain, however the level of increase reaches 5 °C and above for northern continental land masses, up to 5 °C for coastal regions north and up to 4 °C for coastal regions south of 30° *N* until the end of the century. Note, that the changes in daily maximum temperature are statistically significant for all grid cells and over all time periods and scenarios.

3.2.2. Precipitation

While the annual precipitation sum (Fig. 5 (b), left) shows no significant changes through 2099 within RCP scenario 2.6, a moderate increase can be seen for RCP scenario 8.5, reaching + 0.5 mm in the daily sum, respectively + 180 mm for the annual total. Maximum peaks (minimum extremes) within the model range are consistently higher (lower) for RCP 8.5 (RCP 2.6), however the error margin of ±200 mm

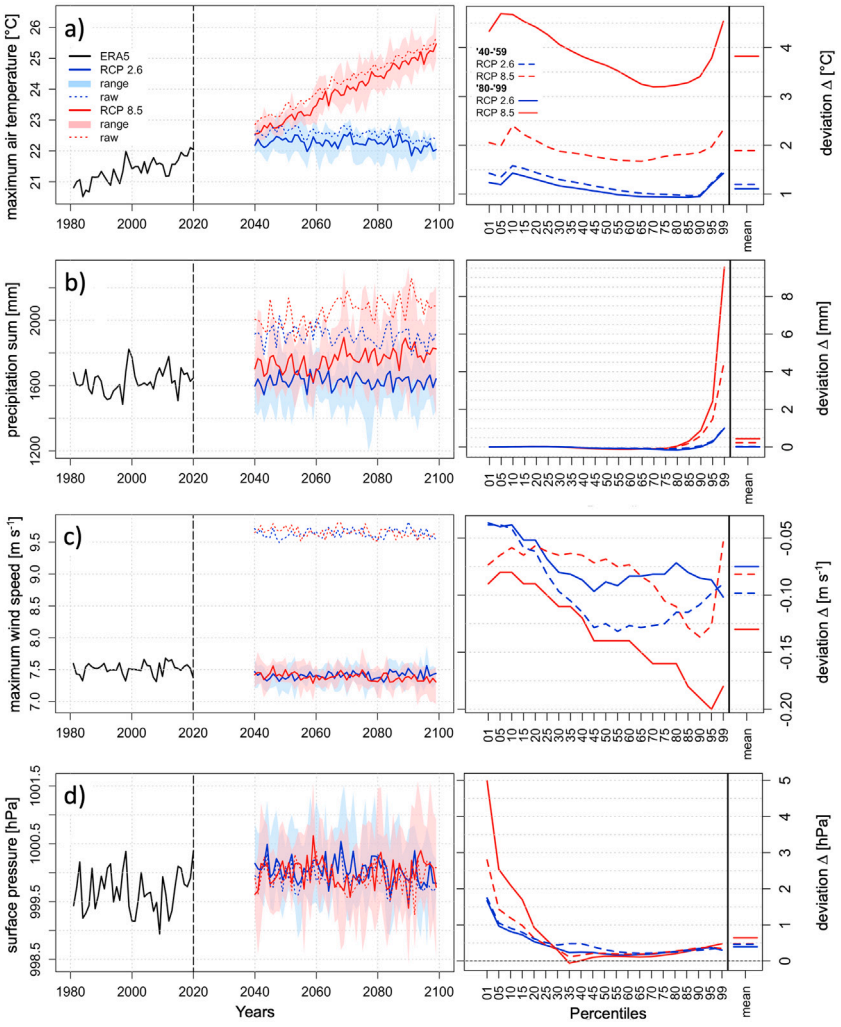

Fig. 5. Left: Future projections of annual mean for (a) maximum temperature, (c) maximum wind speed, (d) surface pressure, and annual sum for (b) precipitation until 2099. ERA5 reference represented by solid black line, RCP 2.6 in blue, RCP 8.5 in red. Dotted lines are raw output, solid lines are model mean of bias adjusted data, shaded areas indicate range of models. Right: Changes in percentiles for 2040–2059 in dashed lines,2080–2099 in solid lines. Each with reference to 1981–2000, model minus ERA5. (For interpretation of the references to colour in this figure legend, the reader is referred to the web version of this article.)

for the annual precipitation sum is high within both scenarios. Regarding changes in the percentile-based thresholds, no significant changes can be seen for low and mid-range daily precipitation events (Fig. 5 (b), right). For heavy precipitation events the models suggest an increase which is stronger the greater the return period. For RCP scenario 2.6 daily precipitation with a return period of 100 days is modelled to be increased by 1 mm. Within RCP scenario 8.5, however, daily precipitation sums with an equal return period are in mean modelled 9.5 mm, or 20%, higher for the period 2080–2099 when referring to 1981–2000. Similar to maximum temperature, precipitation extremes exceeding thresholds above the 95th percentile are simulated to experience a stronger intensification than the overall mean increase, which is 10%.

Notable regional differences in the prediction of future precipitation can be detected (Fig. 7). These changes, however, remain non-significant for many parts of the study region. For the RCP 2.6 scenario a slight drying trend appears for regions within 20°N and 30°N, rarely indicating statistical significance in near-coastal areas. This drying trend is extended southwards over the continent, reaching a decrease in mean daily precipitation of up to −20%. Over Northern China, the South China Sea and the Philippine Sea daily precipitation is to increase by up to 30%. Predicted changes remain persistent for 2040–2059 and 2080–2099. Within the RCP 8.5 scenario variations within central and eastern China appear, mostly reaching significance for decreases in daily precipitation. For 2040–2059, the predictions remain comparable, one exception being maritime areas south of 20°N which inherit a significant increase of up to 20%. In contrast to RCP 2.6, the simulated increase north of 35°N and south of 25°N within RCP scenario 8.5 will intensify until the end of the century and amount up to 30%–50%. Especially south of 25°N the transition line from significant increases in daily precipitation to non-significant variations is embodied by the coastline, affecting mostly southeastern China, Vietnam, Taiwan and the Philippines.

3.2.3. *Maximum wind speed*

The comparison between raw and bias adjusted projections of daily maximum wind speed (Fig. 5(c), left) shows the notable positive bias discussed above (Fig. 3) . The adjusted data shows no particular deviations in future time periods and scenarios from the reference period and the model span is consistently ±0.25 m s^{-1}. Scenario 8.5 shows a tendency towards decreasing maximum wind speeds beginning in 2080. It becomes clear from the percentile-based analysis (Fig. 5 (c), right) that this is mostly contributed to by a decrease in extreme events of

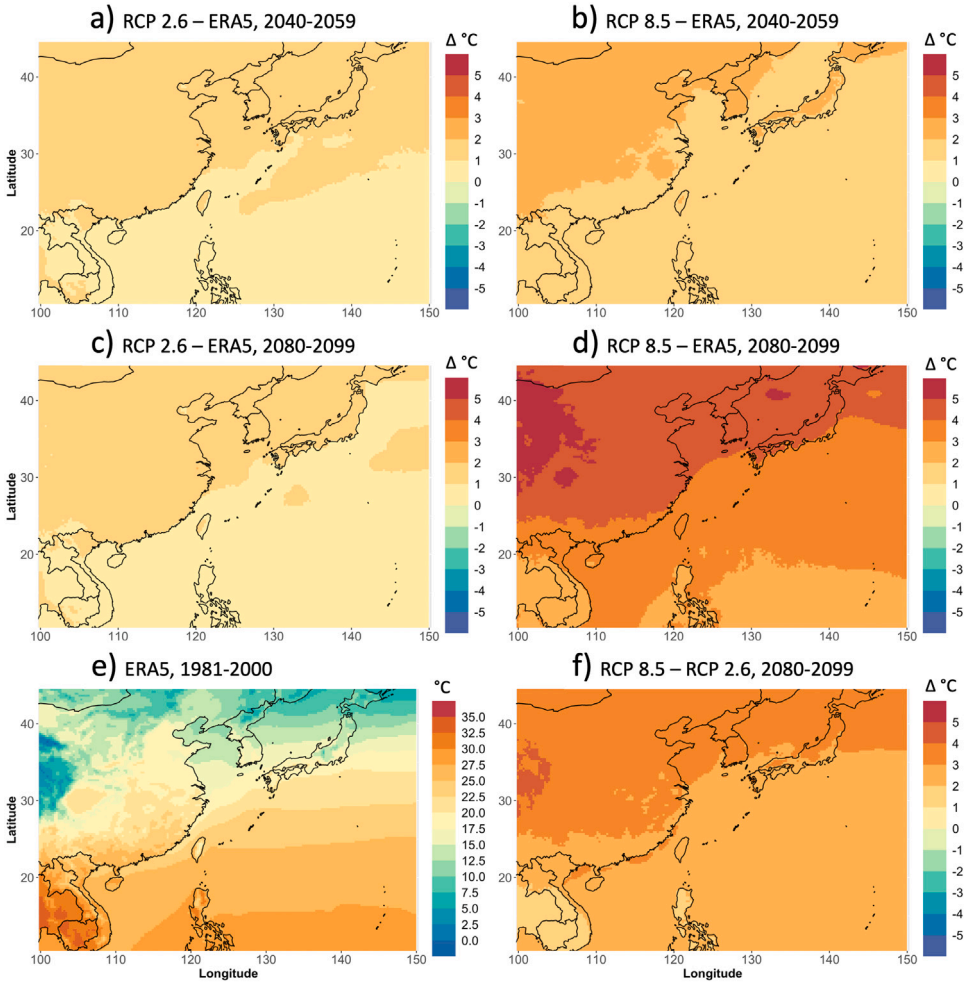

Fig. 6. Changes in mean daily maximum temperature in CORDEX model mean. (a) RCP 2.6 minus ERA5 (2040–2059), (b) RCP 8.5 minus ERA5 (2040–2059), (c) RCP 2.6 minus ERA5 (2080–2099), (d) RCP 8.5 minus ERA5 (2080–2099), (e) ERA5 reference 1981–2000, (f) RCP 8.5 minus RCP 2.6. Dots indicate statistical significance at $\alpha = 0.05$. Note, that all grid cells for (a)-(d) and (f) show statistical significance for maximum temperature.

high wind maxima, reaching to −0.2 m s^{-1} in 2080–2099. Still, the overall level of deviations from the reference period remains low.

The spatial manifestation of the projected changes (Fig. 8) shows similarities to the previous predictors, namely comparable results regarding the two time periods for scenario 2.6 as well as 2040–2059 for the scenario 8.5. For maximum wind speed, most regions north of 25°N are to experience a decrease in wind speed of up to −0.6 m s^{-1}, with regional minima in the Tibetan Plateau, northeastern China and the northern Philippine Sea. While non-significant deviations are predominant in southeastern China, parts of the South China Sea and the Indochinese Peninsula show significant increases in maximum wind speed. During 2080–2099 within the RCP scenario 8.5, the spatial structure remains, yet the changes are further intensified and reach −0.8 m s^{-1} and 0.6 m s^{-1}, respectively. Also, significant increases spread throughout most of the South China Sea and reach the surrounding coastlines.

3.2.4. Surface pressure

When analysing surface pressure, the strong dependence on the geographical altitude must be kept in mind. Discrepancies in the underlying surface altitude for reference and model data impose an additional source of error that is handed to bias adjustment. The long-term analysis (Fig. 5 (d), left) shows a marginal projected change in mean surface pressure for both RCP scenarios and time periods reaching up to +0.6 hPa. The range of models lies within ±0.75–1 hPa. The largest contribution to this change can be attributed to the lowest percentiles (Fig. 5 (d), right), starting with +0.5 hPa for the 30th percentile and reaching up to +5 hPa for the 1st percentile, depending on the time period and scenario. Due to the dependency on altitude these changes rather indicate the location than a change in events, i.e. a change in the regions with the lowest surface pressure.

This assumption is confirmed when the spatial distribution of the projected changes is taken into account (Fig. 9). While for almost the entire domain an increase in surface pressure is projected, the increase over land masses is higher than over maritime areas. For scenario 2.6 projections are consistent until the end of the century and show an increase of up to +0.5 hPa over the ocean and up to +2 hPa over land masses, reaching a maximum over the Tibetan Plateau. For this predictor, too, the spatial structure is similar for both scenarios and the expected changes for scenario 8.5 are amplified. This applies primarily to land masses, for which the expected change reaches +5 hPa for 2080–2099.

3.3. Tropical cyclone-force wind events

The annual frequency of days with tropical cyclone-force winds within the reference period 1981–2000 (Fig. 10) shows a latitudinal

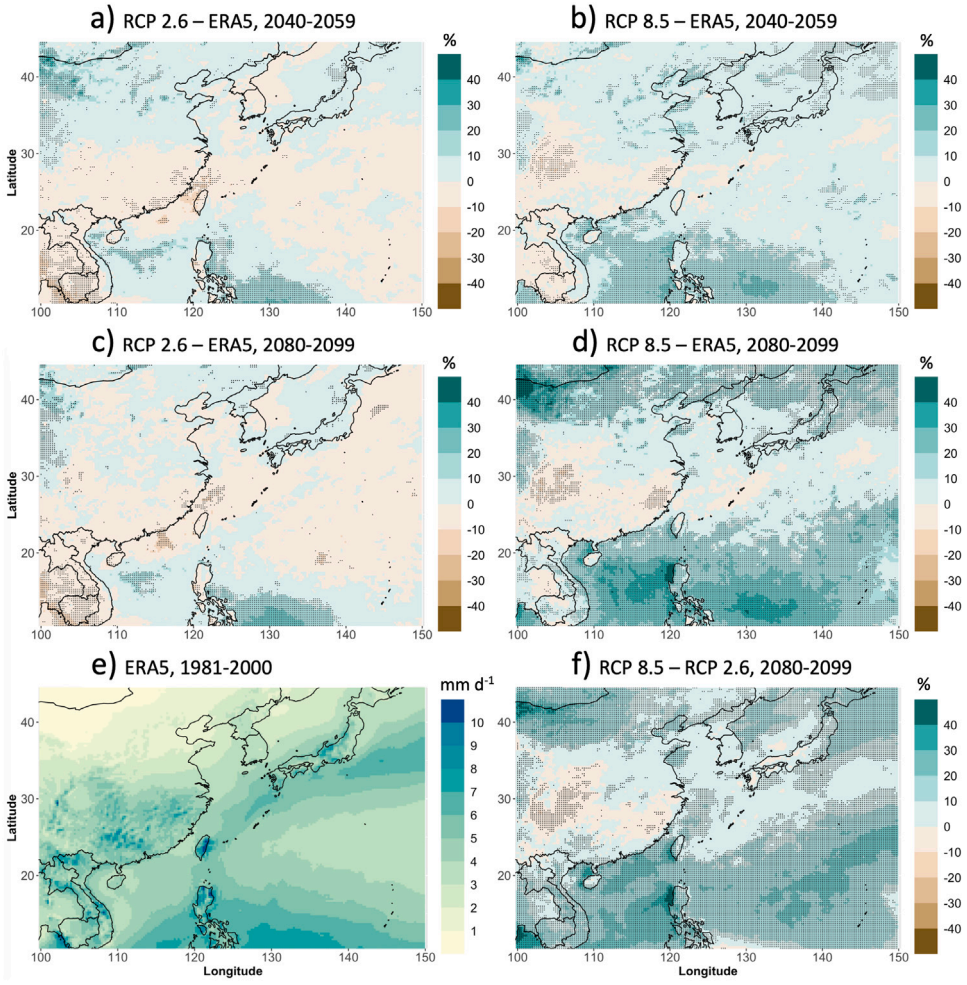

Fig. 7. As Fig. 6, but for mean daily precipitation.

gradient, with low frequencies south of 10°N and reaching up to seven days per year at 20°N, as well as a longitudinal gradient, with increasing frequencies reaching westward from 150°E to 120°E. The maximum frequency of up to 10 days per year occurred in the Luzon Strait and the Taiwan Strait. Within the period 2080–2099 and under the RCP 2.6 scenario, most regions in the eastern half of the domain are modelled to experience a decrease in frequency, yet indicating statistical significance only over the eastern Luzon Strait. Significant increases in the annual frequency are projected for the southern Philippine Sea and extend over the Philippines into the South China Sea and reach the Vietnamese and Chinese coastline. Maximum increases are modelled at +1 to +1.5 days per year. When analysing the RCP 8.5 scenario, the overall spatial structure of the predicted changes remains. An exception to this appears over the Taiwan Strait, where a complex picture of significant increases and decreases for scenario 2.6 changes into overall significant increases for RCP 8.5. For the remaining domain, a general shift including amplified increases and a larger extent of regions with statistically significant increases appears for RCP 8.5, together with weaker changes in regions with a decrease in frequency. The maximum increase in days with tropical cyclone-force winds is +2 days per year and is located in the South China Sea, accounting for an increase of up to 66%.

3.4. Compound events of extreme precipitation and wind

During 1981–2000, the highest number of compound events, according to the underlying definition, occurred north of 15°N, reaching up to three days per year over the South China Sea and 4.5 days over the Philippine Sea (Fig. 11). The annual count rapidly decreases when approaching the shoreline. The spatial pattern of the modelled changes matches the analysis of tropical cyclone-force days, predicting a shift in the region of maximum activity to the west of the Philippines and into the South China Sea. Under RCP 2.6, the projection includes a decrease in the annual frequency for most of the northern and central Philippine Sea, sparsely reaching −2 days and statistical significance. For the southern Philippine Sea statistically significant increases of up to 1.5 days are modelled and reach over the Philippines into the South China Sea and the Chinese and Vietnamese coast. Within RCP 8.5, less regions with a modelled decrease appear and projected increases are amplified. This applies especially to the Taiwan and Luzon Strait, where increases reach up to 2 days per year, as well as the South China Sea, of which most regions are to experience a significant increase in compound events, with maximum increases reaching up to three per year. Note, that the projected increases reach significantly further into the land masses and that coastal areas of China and Vietnam are stronger affected by changes in compound events than for solely wind-based events. While this already applies for RCP 2.6, the effect is significantly amplified under RCP 8.5.

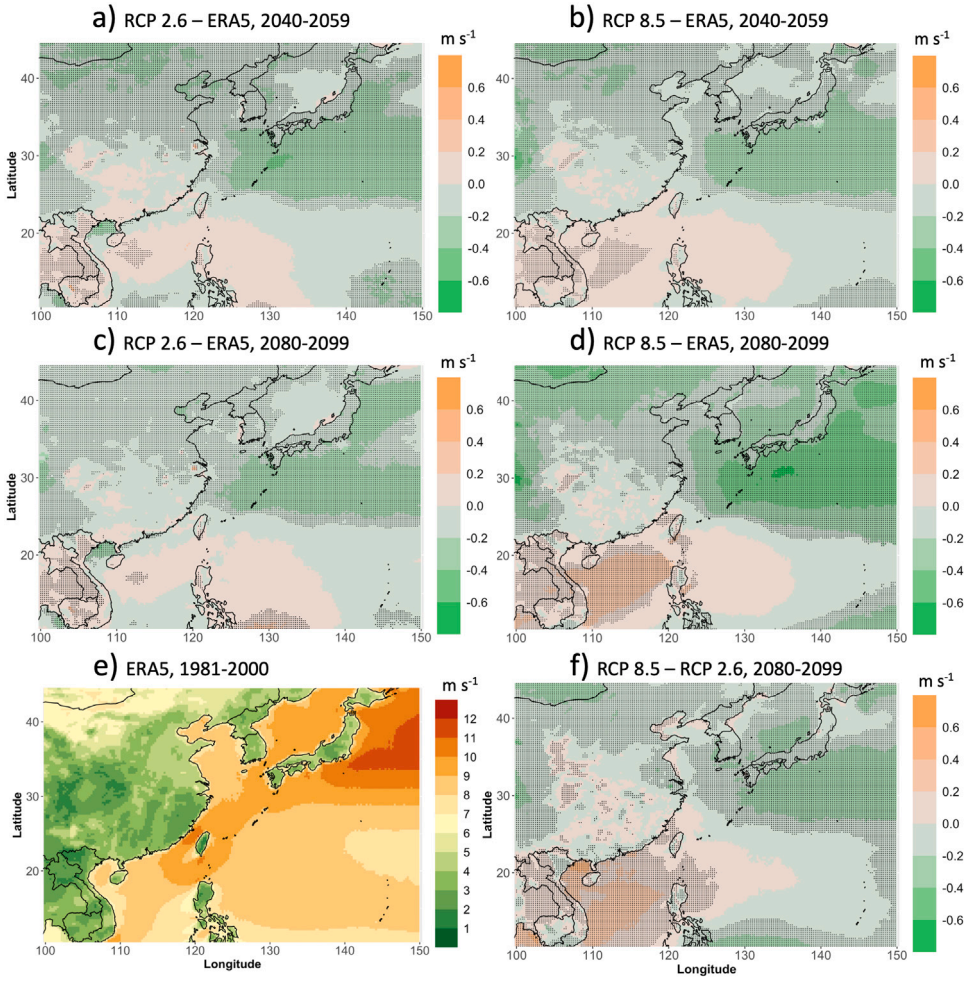

Fig. 8. As Fig. 6, but for mean daily maximum wind speed.

4. Discussion

In the following section the described results are discussed and contextualized. The structure of presentation remains, therefore addressing the assessed uncertainties and applied bias adjustment methods first. The validity of results regarding long-term climate change, changes in univariate extreme events and changes in compound extreme events are discussed in the following. The section is concluded by discussing limitations linked to the analysis.

4.1. Bias adjustment

Results show that the raw model output quality is strongly dependent on the inspected variable and the chosen GCM-RCM combination. The model mean of the raw data potentially exceeding the model range of the bias adjusted models proves the necessity of applying bias adjustment methods, of which quantile delta mapping provides the most accurate results within cross validation for our study. As Laux et al. (2021) demonstrated, the quality of an analysis can be improved by including more than one bias adjustment method into an ensemble. Taking this into account we applied multiple correction methods, however the bias resulting from smoothing spline-based corrections was inherited in the ensemble, affecting the data quality negatively. While long-term evaluation metrics, e.g. BIAS and percentile-based thresholds, prove QDM to perform a nearly optimal correction of bias, metrics including daily variability, e.g. MAE, RMSE, and correlation, show no notable improvement. As we included the GCM-driven historical experiments provided by CORDEX to assess the joint bias from the consulted GCM and RCM, this result is expected due to no temporal correspondence between the model output and ERA5. In the context of a long-term climatological analysis, however, day-to-day variability becomes inferior the quality of long-term metrics and therefore conclusions drawn from the analysis of the bias adjusted data are of high value. For the analysis of daily events, e.g. compound events, the remaining bias has a potential impact on the accurate definition of events and must therefore be taken into account. Nevertheless, as QDM improves the model data to inherit an overall BIAS of nearly 0, the assumption of neither systematic nor significant over- or underestimations (see also Section 3.1) can be upheld, increasing the validity of event-based analyses on a daily basis. This, as is common within climatological analyses, follows the assumption that the general physical relationships within the earth system remain unchanged in the future.

4.2. Long-term climate change

The results regarding projected long-term changes of the inspected predictors in general are in accordance with findings of similar studies and the summaries of the (IPCC, 2021). Of particular interest, in terms

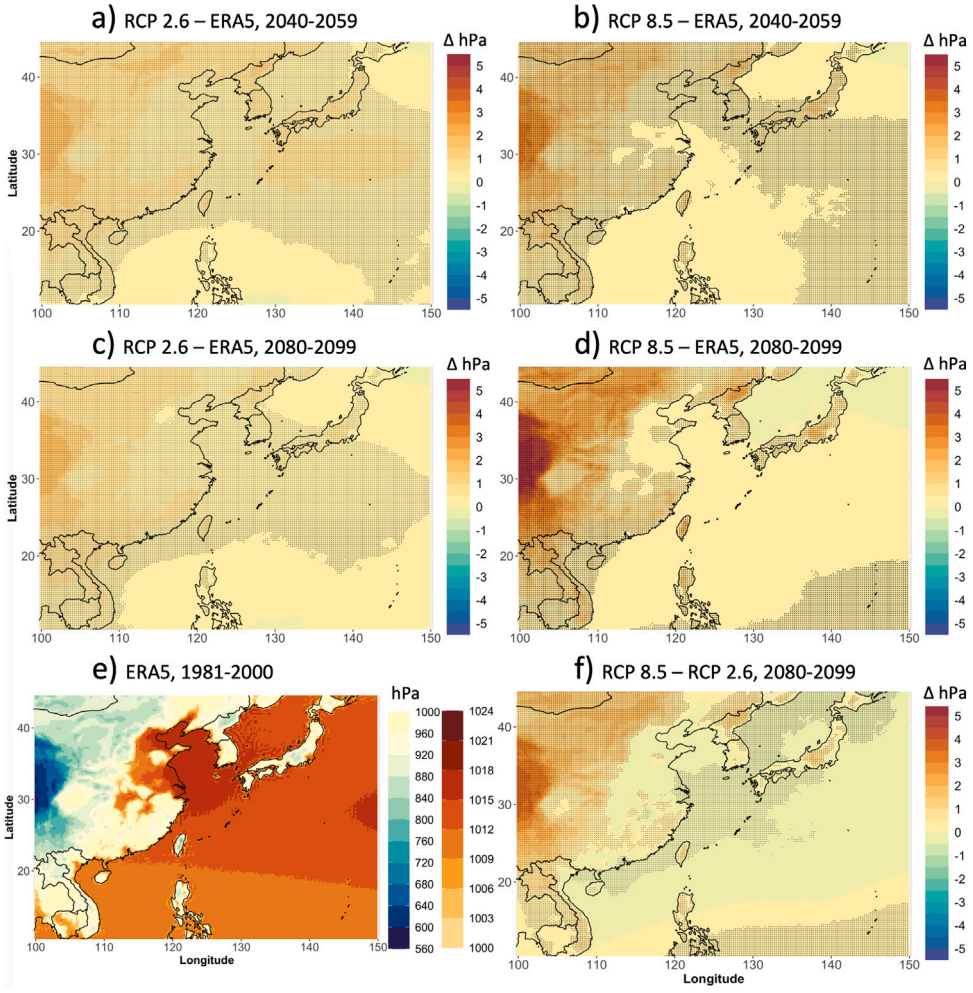

Fig. 9. As Fig. 6, but for mean daily surface pressure.

of daily maximum temperature, is the prevailing increase until the mid-21st century for all provided RCP scenarios and the level of severity for the 8.5 scenario until 2099. While heat extremes already impose a remarkable threat to the environment and human health today (Zhang et al., 2017; Lu and Chen, 2016; Bao et al., 2016; Gasparrini et al., 2015; Ma et al., 2014), a further intensification of heat extremes must be closely monitored and mitigated to avert additional costs and losses. The amplified increase in daily maximum temperatures above the 95th percentile adds to this risk.

A variety of studies prove difficulties and challenges when projecting precipitation, attributing large uncertainties to, for example, the model resolution, model parameterizations, and local specifics models are not capable of reproducing (Huang et al., 2013; Chen and Frauenfeld, 2014). These uncertainties are reflected in the raw data used in this study and can, to a considerable extent, be reduced by applying bias adjustment. While the model mean particularly indicates significant increases over the South China Sea and the Philippine Sea and significant deviations between the RCP scenarios 2.6 and 8.5, a large inter-model spread remains, partially including opposing signals of change for different GCM-RCM combinations under the same RCP scenario. This must also be taken into account when analysing daily extremes. However, we prove quantile delta mapping to reduce the margin of error for specific percentiles of extreme precipitation. In this context, the aforementioned potential increase in daily extreme precipitation of up to 9.5 mm under RCP 8.5 stands out. It will also be of high relevance how the significant precipitation increases over the South China Sea will have an influence on the adjacent coastal regions and how far these changes will reach into the continental areas. While potential changes in precipitation frequency and intensity have also been discussed in previous studies (Gan et al., 2022; Li et al., 2021; Zhang and Zhou, 2020; Chen et al., 2017; Sun and Ao, 2013), further improvement in the precision of projections is necessary to grant the foundation of appropriate and sufficient adaptive measures. In this context, our study contributes further insights into regional differences and noteworthy uncertainties within the provided projections of future precipitation.

For the largest part of the study region, projected increases in surface pressure are accompanied by decreases in daily maximum wind speed, which is plausible from a physical point of view. This includes a negative correlation between air temperature and near-surface wind speed (Wu et al., 2018) as well as reduced near-surface wind speeds due to a reduction of the pressure gradient force (Wu et al., 2016; Guo et al., 2011). However, these authors also determine that a regional distinction becomes necessary when analysing near-surface winds, as the outlined predictors alone do not sufficiently explain observed changes on this height level. This also applies to the findings of our study that indicate a significant increase in daily maximum wind speeds across the South China Sea, accompanied with an increase in the annual frequency of extreme wind events and compound events.

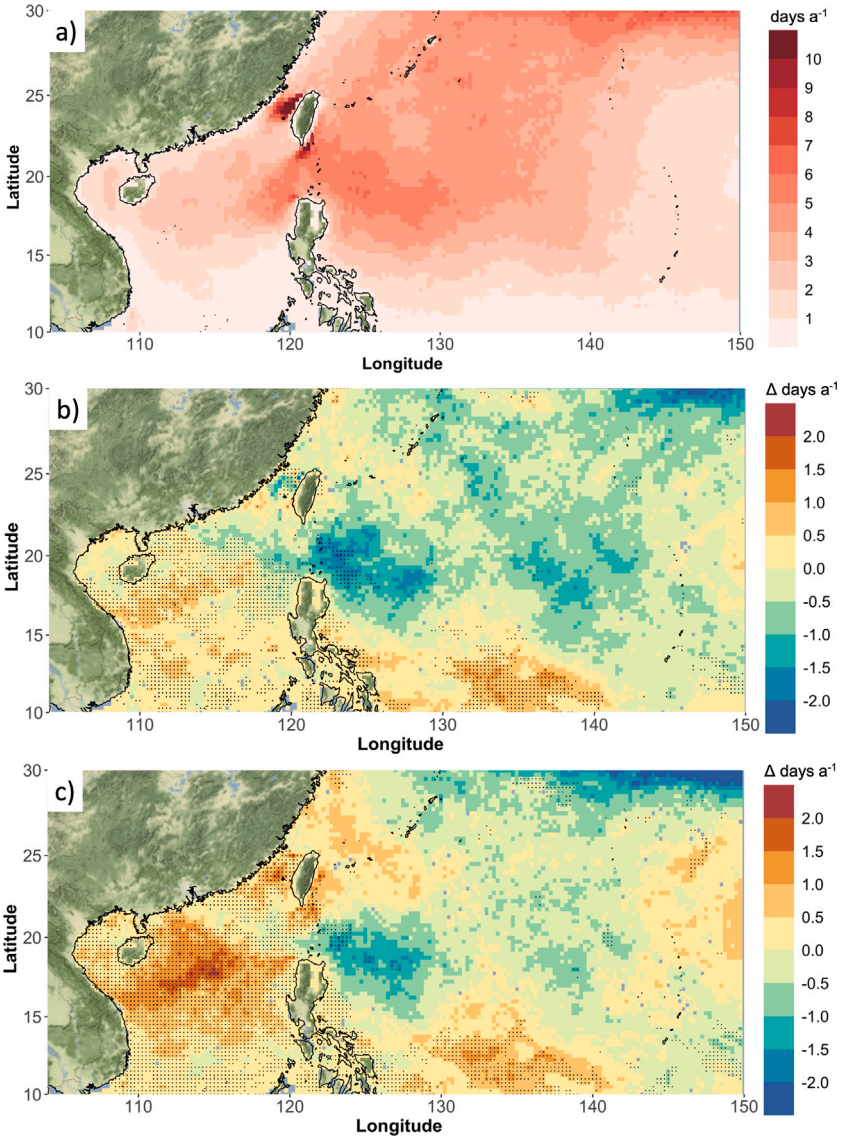

Fig. 10. Annual frequency of days with tropical cyclone-force winds >17.5 m s^{-1}. (a) ERA5 1981–2000, (b) projected changes in 2080–2099 for CORDEX model mean under RCP 2.6, (c) projected changes in 2080–2099 for CORDEX model mean under RCP 8.5. Dots indicate statistical significance at $\alpha = 0.05$.

4.3. Wind-based extreme events and compound events

Two main findings emerge from this analysis in terms of wind-based extreme events and compound events of extreme wind speeds and heavy precipitation. For one, predictions show a distinct westward shift of the area with the highest annual frequency, from the Northern Philippine Sea into the South China Sea. This appears for both RCP scenarios, but increases are amplified under RCP 8.5 conditions and statistically significant increases are more widespread. On the other hand, these changes appear not only over maritime areas, but reach into the continent, substantially impacting coastal regions. For most of these regions, the inspected compound events occurred less frequently than extreme events including only wind. Under the given scenarios, especially under RCP 8.5, the projected relative increases in the annual number of compound events exceeds those of univariate wind-based extreme events. As pointed out by Zhang et al. (2021), and Zscheischler et al. (2018), the impacts of compound events on the environment, economy and human health are disproportionate when compared to univariate extreme events. Protective and adaptive measures counteracting these additional risk factors become even more necessary if the frequency of compound events increases under future climate conditions.

Regarding the question whether the projected long-term changes in these predictors act favourable towards tropical cyclogenesis, the complex physical relations and interactions act detrimental towards a clear interpretation. On the one side, increased radiation and near-surface air temperatures, interacting with sea surface temperatures, enhance the development of tropical cyclones (Emanuel, 2007). On the other side, Vecchi and Soden (2007) show adverse effects of increased upper-tropospheric warming and wind shear towards tropical cyclogenesis. To grant a more comprehensive view, further investigations of additional predictors would become necessary but exceeded the scope of our analysis. This can be subject to further studies, that can potentially make use of further improved datasets, for example in terms of grid resolution, parameterizations and computational capacity.

Taking the projected changes of the atmosphere into account, Knutson et al. (2015) show a potential decrease in the overall frequency of

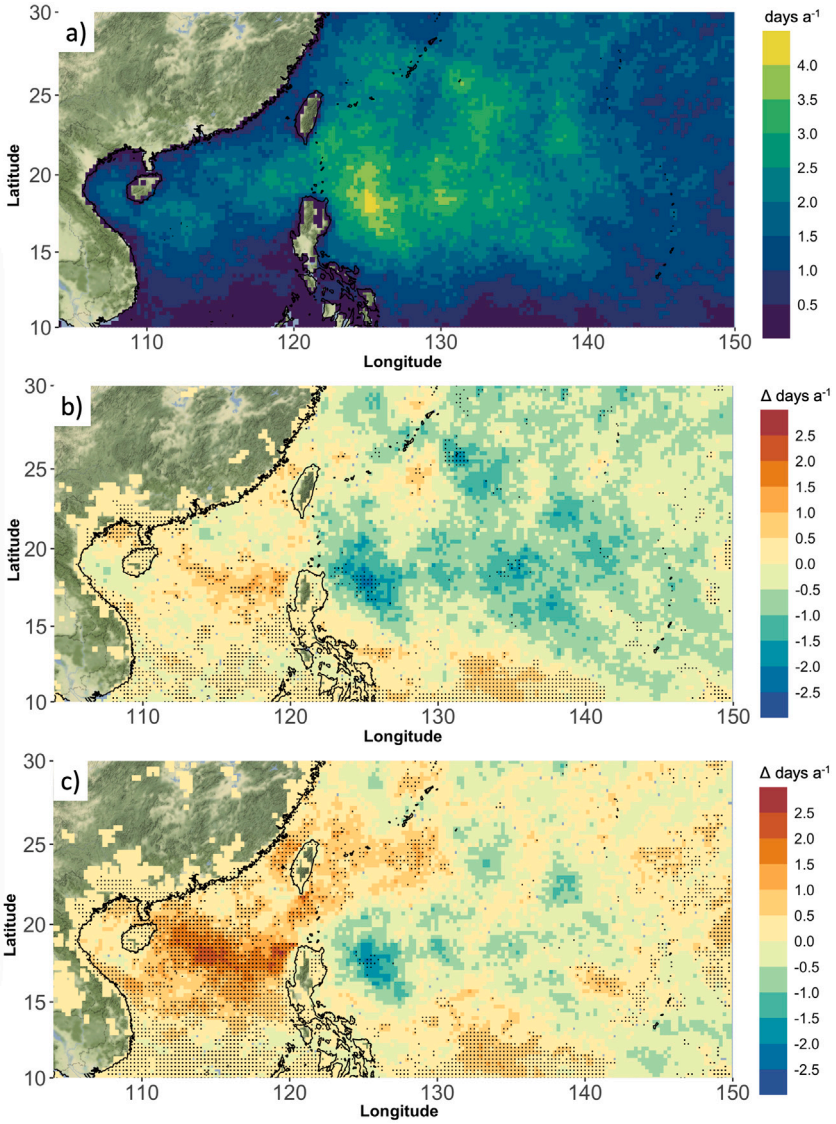

Fig. 11. Annual frequency of compound extreme events including tropical cyclone-force winds (>17.5 m s^{-1}) and daily precipitation above the 99th percentile (maximum 1 day lag). (a) ERA5 1981–2000, (b) projected changes in 2080–2099 for CORDEX model mean under RCP 2.6, (c) projected changes in 2080–2099 for CORDEX model mean under RCP 8.5. Dots indicate statistical significance at $\alpha = 0.05$.

tropical cyclones, but an increase in storm intensity and precipitation. In its latest Assessment Report, the (IPCC, 2021) discusses an increase in precipitation and storm intensity to be the likely future scenario and anthropogenic warming to be one of the main drivers. While our study mostly confirms these projections, it can contribute to the existing expertise by showing the necessity of a regionally differentiated analysis. While large portions of our study area are projected to experience a decrease in wind-based extreme events and compound events, specific subregions, e.g. the coastal regions of the South China Sea, show significant increases pointing out potentially heavy socioeconomic impacts in the future.

4.4. Limitations

While we thoroughly accounted for uncertainties in the underlying data sets, limitations regarding the interpretation of the results remain. For example, the impact of the applied interpolation method to match the spatial structures of the model and evaluation data should be further investigated. As the analyses of Latombe et al. (2018) and Accadia et al. (2003) pointed out, the choice of interpolation method can impact the data quality negatively and impose an additional source of bias.

To further evaluate the potential of bias adjustment in our study region, additional methods, as for example discussed in Gutiérrez et al. (2019), could be included and compared to this research. Also, multivariate (Dieng et al., 2022; Cannon, 2018), trend-preserving bias adjustment methods (Lange, 2019) could be applied in this context. This continuative analysis could, for example, highlight uncertainties due to undetectable changes in trends within future periods.

It will also be of interest to study uncertainties arising from the choice of reference data set. Regarding this issue (Xu et al., 2022a), prove ERA5 to be a reliable reference for our study region. However, the authors also point out potential sources of bias within reanalysis. For example, the inclusion of station-based observational data sets may lead to altitude-related discrepancies between the station data and the final reanalysis product. In the context of uncertainties arising from

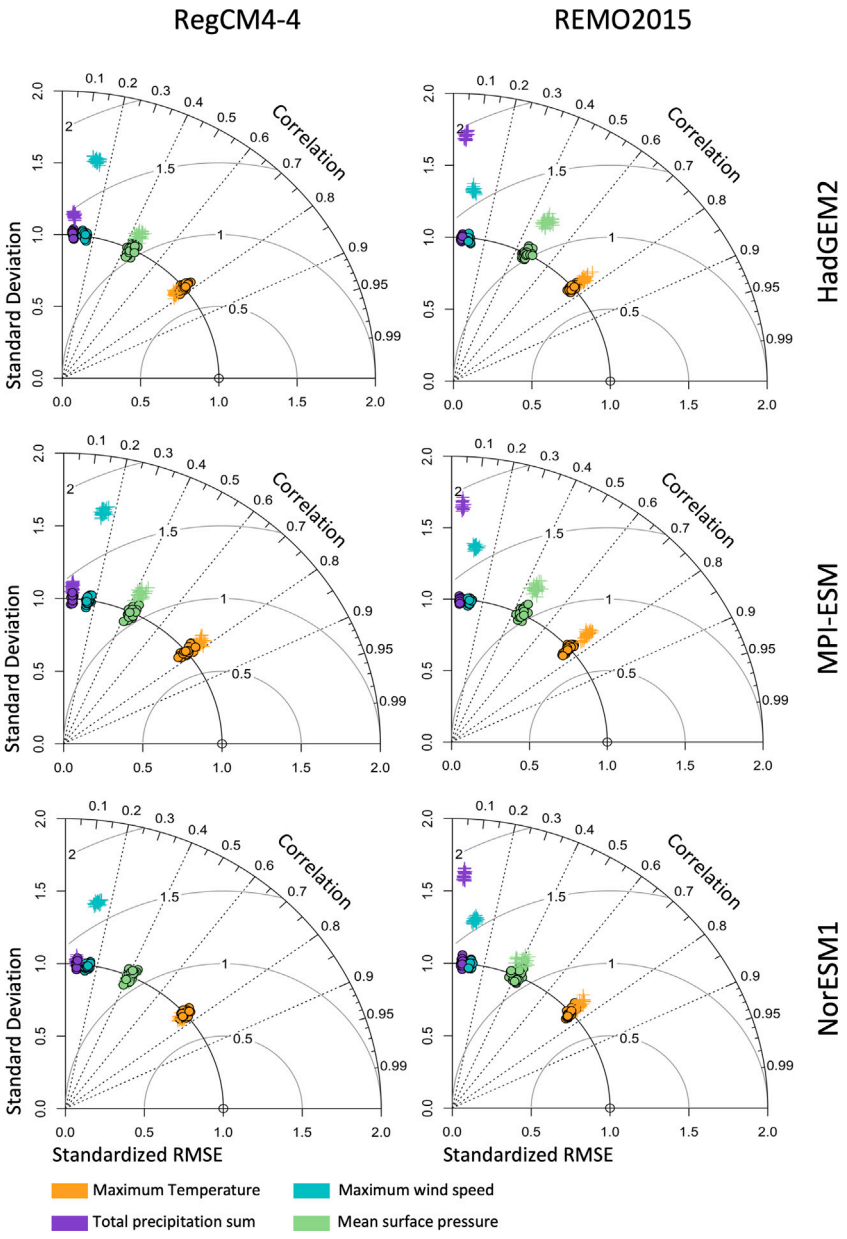

Fig. A.1. Taylor diagrams to evaluate 30 cross validated ensemble members used for quantile delta mapping (QDM). Each object represents one ensemble member, black outlines depict members of the adjusted data set, colours refer to the inspected variables. (For interpretation of the references to colour in this figure legend, the reader is referred to the web version of this article.)

model characteristics a discrimination of bias originating from the GCMs and the RCMs can furthermore be achieved by including RCM runs driven by reanalysis (Tang et al., 2022; Pastén-Zapata et al., 2020; Martynov et al., 2013).

In terms of wind-based extreme events and compound events, this study is heavily reliant on the findings of Walsh et al. (2007) regarding the definition of tropical cyclone-force winds. While extensive research exists towards the ability of models to represent tropical cyclones sufficiently and studies demonstrate constraints under which such an analysis becomes plausible, it nevertheless remains a source of uncertainty. Therefore, this research could be complemented by a continuative uncertainty assessment, for instance concerning the choice of thresholds regarding extreme events. In the case of precipitation, for example, the 98th percentile (Martius et al., 2016; Guzzetti et al., 2008), and the 95th percentile (Zhang et al., 2011; Cao et al., 2018) could be considered. As Zscheischler et al. (2021) demonstrated, a deeper statistical analysis can also reveal changes in the statistical dependence of two compounding variables. This was beyond the limits of this study but could be of high interest and grant further insights into potential future atmospheric mechanics.

While the findings of this study provide a comprehensive overview of possible atmospheric changes in the future, the spatial resolution of the results could be improved to obtain optimized projections for stakeholders and decision-makers on site. A refinement and further evaluation of these findings could be achieved, for example with focus on urban regions such as Shanghai and Shenzhen, by performing statistical downscaling and including station-based observations.

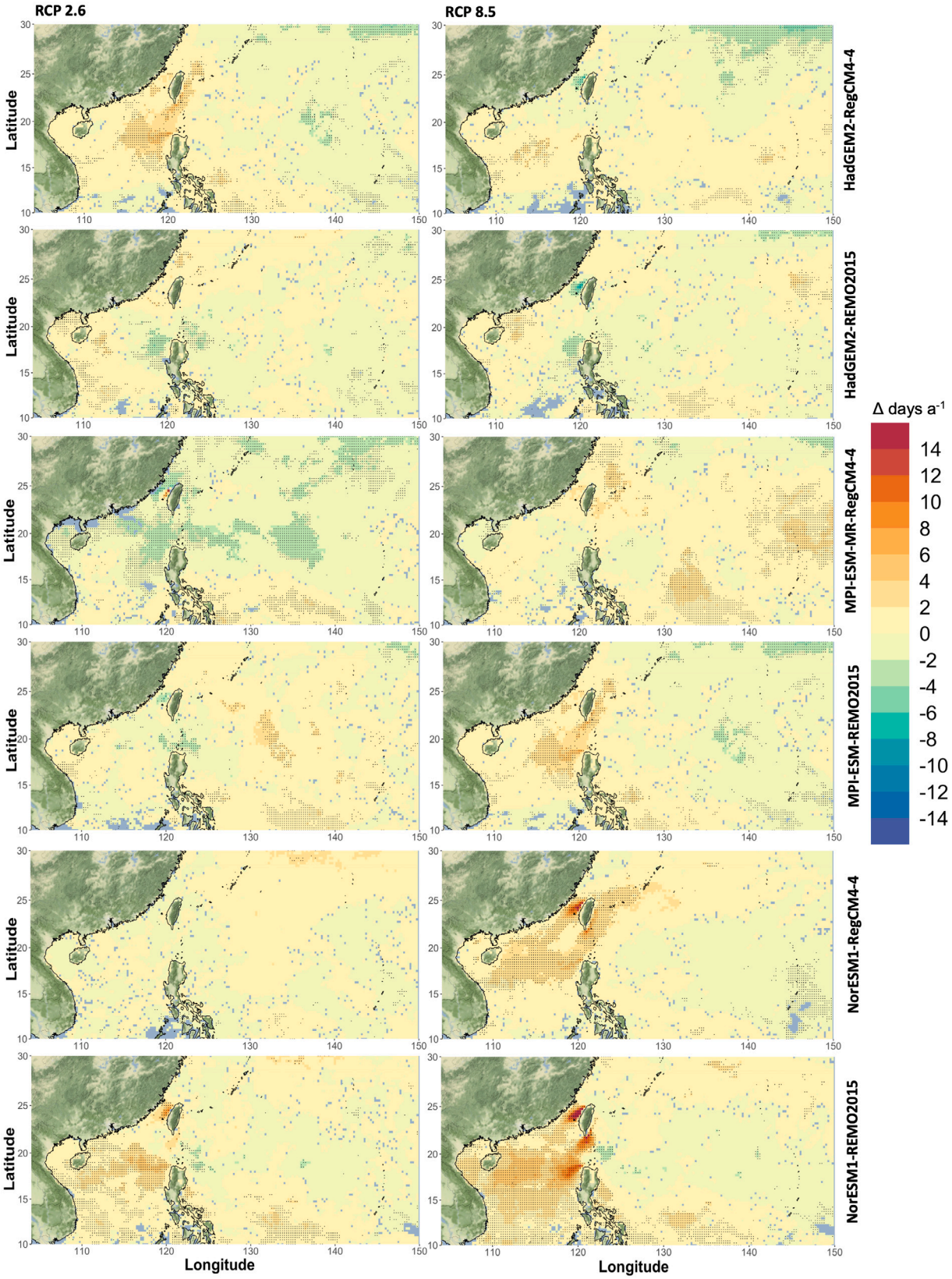

Fig. B.1. Projected changes in the annual frequency of days with tropical cyclone-force winds >17.5 m s^{-1} for the included single models. Left side: projected changes in 2080–2099 under RCP 2.6, right side: projected changes in 2080–2099 under RCP 8.5. Rows are single models in accordance with Table 1. Dots indicate statistical significance at $\alpha = 0.05$. Please note the varying colour scale when comparing to Fig. 10.

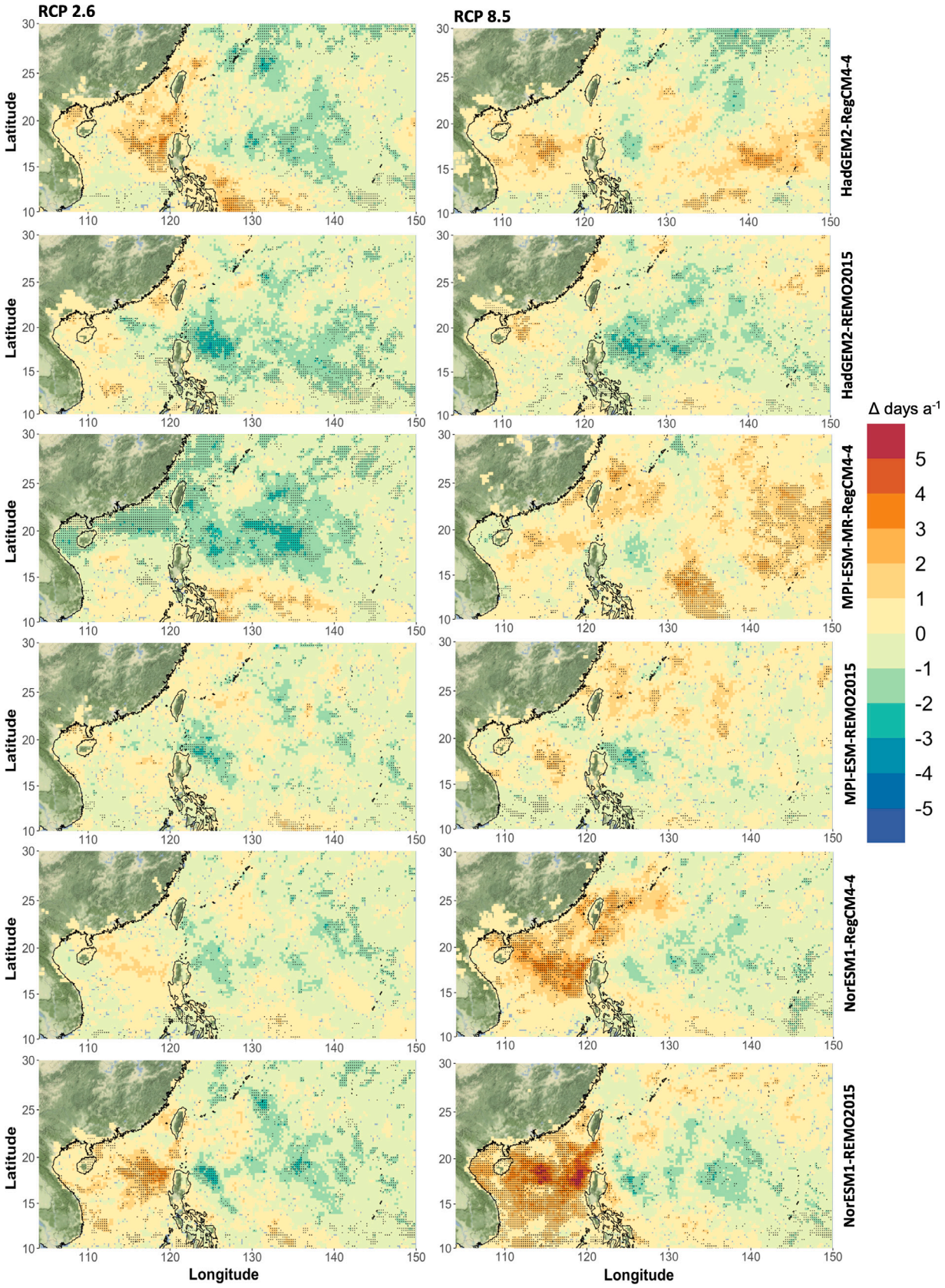

Fig. C.1. Projected changes in the annual frequency of compound extreme events including tropical cyclone-force winds (>17.5 m s^{-1}) and daily precipitation above the 99th percentile for the included single models. Left side: projected changes in 2080–2099 under RCP 2.6, right side: projected changes in 2080–2099 under RCP 8.5. Rows are single models in accordance with Table 1. Dots indicate statistical significance at $\alpha = 0.05$. Please note the varying colour scale when comparing to Fig. 11.

5. Conclusions

The objectives of this study included performance assessment of bias adjustment methods, long-term changes in crucial atmospheric predictors under different future scenarios, and projected changes in extreme and compound events over East Asia and the northwest Pacific. To address these objectives we created a multi-model multi-scenario ensemble based on different bias adjustment methods and GCM-RCM combinations obtained from EAS-CORDEX. The key findings, with regard to the research questions, include the following:

Quantile delta mapping performs best in minimizing bias and proves to be a valid method to optimize the quality of model output and improve the robustness of the projected atmospheric changes. Statistically significant differences exist between the debiased projections of RCP scenarios 2.6 and 8.5, and this is valid for large portions of the study area. Large differences also exist between the bias adjusted output of the included single models with partly contradictory trends for specific parameters and regions. These two factors indicate the range of uncertainty that must be considered when using these data sets as basis for further research or decision making.

The most important long-term changes in the inspected model mean values include an increase in daily maximum temperature ranging from 1.5 to 4 °C, dependent on the future socioeconomic and technological development. Annual precipitation projections include a slight increase for RCP 8.5, however the range of uncertainty remains high. The picture is uncertain for maximum wind speed and surface pressure, mostly being dominated by non-significant variations. For maximum temperature and precipitation, percentile-based daily extreme events on the heavy tail of the distribution are projected to intensify more rapidly than the overall mean.

The analysis of univariate extremes and compound events necessarily requires a regional distinction. While many subregions, solely over the ocean, will experience a decrease in frequency, specific parts of the study domain show a significant increase in both wind-based extremes and compound events. This relates in particular to the South China Sea, for which both types of events are projected to increase in frequency and intensity. In this region, the relative increase in relation to the annual frequency is projected to be higher for compound events than for solely wind-based events, and the expected changes are amplified under RCP 8.5.

CRediT authorship contribution statement

Patrick Olschewski: Conceptualization, Data curation, Formal analysis, Investigation, Code, Writing – original draft, Writing – review & editing. **Patrick Laux:** Conceptualization, Data curation, Formal analysis, Investigation, Project administration, Supervision, Writing – review & editing. **Jianhui Wei:** Conceptualization, Data curation, Formal analysis, Investigation, Project administration, Supervision, Writing – review & editing. **Brian Böker:** Formal analysis, Investigation, Code, Writing – review & editing. **Zhan Tian:** Conceptualization, Project administration, Supervision, Writing – review & editing. **Laixiang Sun:** Conceptualization, Project administration, Supervision, Writing – review & editing. **Harald Kunstmann:** Conceptualization, Project administration, Supervision, Writing – review & editing.

Declaration of competing interest

The authors declare that they have no known competing financial interests or personal relationships that could have appeared to influence the work reported in this paper.

Data availability

The obtained ERA5 reanalysis data is openly accessible via the Climate Data Store of the European Centre for Medium-Range Weather Forecasts (ECMWF) under the following link: https://cds.climate.copernicus.eu/cdsapp#!/dataset/reanalysis-era5-pressure-levels?tab=overview. CORDEX regionally downscaled model data was obtained from the ESGF Node provided by DKRZ (Deutsches Klimarechenzentrum), which is accessible at https://esgf-data.dkrz.de/search/esgf-dkrz/ upon registration.

Acknowledgements

The major part of this analysis was performed using the programming environment R, version 4.1.1 (R. Core Team, 2017). NetCDF data was processed using the "hyfo" package (Xu, 2020) and the R framework "climate4R", provided by Santander Meteorology Group (Iturbide et al., 2018). R packages "qmap" (Gudmundsson et al., 2012) and "QDM" (Cannon et al., 2015) were consulted for the adjustment of bias. The computationally expensive forming of the cross-validated ensemble members for each bias adjustment method was conducted using the programming environment Julia (Bezanson et al., 2017). We acknowledge the provision of the CORDEX and ERA5 data that was used in this study.

Financial support

This study was conducted in the framework of the Sino-German project Mitigating the Risk of compound extreme Flooding events *MitRiskFlood*, jointly funded by MOST (grant number 2019YFE0124800) and the German Ministry of Education and Research (BMBF) (grant number 01LP2005A).

Appendix A

See Fig. A.1.

Appendix B

See Fig. B.1.

Appendix C

See Fig. C.1.

References

Accadia, C., Mariani, S., Casaioli, M., Lavagnini, A., Speranza, A., 2003. Sensitivity of precipitation forecast skill scores to bilinear interpolation and a simple nearest-neighbor average method on high-resolution verification grids. Weather Forecast. 18 (5), 918–932. http://dx.doi.org/10.1175/1520-0434(2003)018<0918:SOPFSS>2.0.CO;2.

Balica, S.F., Wright, N.G., van der Meulen, F., 2012. A flood vulnerability index for coastal cities and its use in assessing climate change impacts. Nat. Hazards 64 (1), 73–105. http://dx.doi.org/10.1007/s11069-012-0234-1.

Bao, J., Wang, Z., Yu, C., Li, X., 2016. The influence of temperature on mortality and its lag effect: a study in four Chinese cities with different latitudes. BMC Public Health 16 (1), 375. http://dx.doi.org/10.1186/s12889-016-3031-z.

Bengtsson, L., Hodges, K.I., Esch, M., 2007. Tropical cyclones in a T159 resolution global climate model: comparison with observations and re-analyses. Tellus A: Dyn. Meteorol. Oceanogr. 59 (4), 396–416. http://dx.doi.org/10.1111/j.1600-0870.2007.00236.x.

Bentsen, M., Bethke, I., Debernard, J.B., Iversen, T., Kirkevag, A., Seland, O., Drange, H., Roelandt, C., Seierstad, I.A., Hoose, C., Kristjánsson, J.E., 2013. The norwegian earth system model, NorESM1-M – part 1: Description and basic evaluation of the physical climate. Geosci. Model Dev. 6 (3), 687–720. http://dx.doi.org/10.5194/gmd-6-687-2013.

Bezanson, J., Edelman, A., Karpinski, S., Shah, V.B., 2017. Julia: A fresh approach to numerical computing. SIAM Rev. 59 (1), 65–98. http://dx.doi.org/10.1137/141000671.

Boé, J., Terray, L., Habets, F., Martin, E., 2007. Statistical and dynamical downscaling of the seine basin climate for hydro-meteorological studies. Int. J. Climatol. 27 (12), 1643–1655. http://dx.doi.org/10.1002/joc.1602.

Cannon, A.J., 2018. Multivariate quantile mapping bias correction: an N-dimensional probability density function transform for climate model simulations of multiple variables. Clim. Dynam. 50 (1–2), 31–49. http://dx.doi.org/10.1007/s00382-017-3580-6.

Cannon, A.J., Sobie, S.R., Murdock, T.Q., 2015. Bias correction of GCM precipitation by quantile mapping: How well do methods preserve changes in quantiles and extremes? J. Clim. 28 (17), 6938–6959. http://dx.doi.org/10.1175/JCLI-D-14-00754.1.

Cao, F., Gao, T., Dan, L., Ma, Z., Yang, X., Yang, F., 2018. Contribution of large-scale circulation anomalies to variability of summer precipitation extremes in northeast China. Atmospheric Sci. Lett. 19 (12), e867. http://dx.doi.org/10.1002/asl.867.

Carrassi, A., Bocquet, M., Bertino, L., Evensen, G., 2018. Data assimilation in the geosciences: An overview of methods, issues, and perspectives. WIREs Clim. Chang. 9 (5), http://dx.doi.org/10.1002/wcc.535.

Chai, T., Draxler, R.R., 2014. Root mean square error (RMSE) or mean absolute error (MAE)? – arguments against avoiding RMSE in the literature. Geosci. Model Dev. 7 (3), 1247–1250. http://dx.doi.org/10.5194/gmd-7-1247-2014.

Chakraborty, D., Dobor, L., Zolles, A., Hlásny, T., Schueler, S., 2021. High-resolution gridded climate data for Europe based on bias-corrected EURO-CORDEX: The ECLIPS dataset. Geosci. Data J. 8 (2), 121–131. http://dx.doi.org/10.1002/gdj3.110.

Chen, L., Frauenfeld, O.W., 2014. A comprehensive evaluation of precipitation simulations over China based on CMIP5 multimodel ensemble projections. J. Geophys. Res.: Atmos. 119 (10), 5767–5786. http://dx.doi.org/10.1002/2013JD021190.

Chen, H.-P., Sun, J.-Q., Li, H.-X., 2017. Future changes in precipitation extremes over China using the NEX-GDDP high-resolution daily downscaled data-set. Atmospheric Ocean. Sci. Lett. 10 (6), 403–410. http://dx.doi.org/10.1080/16742834.2017.1367625.

Choudhary, A., Dimri, A.P., 2019. On bias correction of summer monsoon precipitation over India from CORDEX-SA simulations. Int. J. Climatol. 39 (3), 1388–1403. http://dx.doi.org/10.1002/joc.5889.

Collins, W.J., Bellouin, N., Doutriaux-Boucher, M., Gedney, N., Halloran, P., Hinton, T., Hughes, J., Jones, C.D., Joshi, M., Liddicoat, S., Martin, G., O'Connor, F., Rae, J., Senior, C., Sitch, S., Totterdell, I., Wiltshire, A., Woodward, S., 2011. Development and evaluation of an earth-system model – HadGEM2. Geosci. Model Dev. 4 (4), 1051–1075. http://dx.doi.org/10.5194/gmd-4-1051-2011.

CORDEX, 2022. Region 7: East Asia. URL https://cordex.org/domains/region-7-east-asia/.

Cornes, R.C., van der Schrier, G., van den Besselaar, E.J.M., Jones, P.D., 2018. An ensemble version of the E-OBS temperature and precipitation data sets. J. Geophys. Res.: Atmos. 123 (17), 9391–9409. http://dx.doi.org/10.1029/2017JD028200.

Dee, D.P., Uppala, S.M., Simmons, A.J., Berrisford, P., Poli, P., Kobayashi, S., Andrae, U., Balmaseda, M.A., Balsamo, G., Bauer, P., Bechtold, P., Beljaars, A.C., van de Berg, L., Bidlot, J., Bormann, N., Delsol, C., Dragani, R., Fuentes, M., Geer, A.J., Haimberger, L., Healy, S.B., Hersbach, H., Hólm, E.V., Isaksen, L., Kållberg, P., Köhler, M., Matricardi, M., Mcnally, A.P., Monge-Sanz, B.M., Morcrette, J.J., Park, B.K., Peubey, C., de Rosnay, P., Tavolato, C., Thépaut, J.N., Vitart, F., 2011. The ERA-interim reanalysis: Configuration and performance of the data assimilation system. Q. J. R. Meteorol. Soc. 137 (656), 553–597. http://dx.doi.org/10.1002/qj.828.

Deque, M., 2007. Frequency of precipitation and temperature extremes over France in an anthropogenic scenario: Model results and statistical correction according to observed values. Glob. Planet. Change 57 (1–2), 16–26. http://dx.doi.org/10.1016/j.gloplacha.2006.11.030.

Dieng, D., Cannon, A.J., Laux, P., Hald, C., Adeyeri, O., Rahimi, J., Srivastava, A.K., Mbaye, M.L., Kunstmann, H., 2022. Multivariate bias-correction of high-resolution regional climate change simulations for west Africa: Performance and climate change implications. J. Geophys. Res.: Atmos. 127 (5), http://dx.doi.org/10.1029/2021JD034836.

Eden, J.M., Widmann, M., Grawe, D., Rast, S., 2012. Skill, correction, and downscaling of GCM-simulated precipitation. J. Clim. 25 (11), 3970–3984. http://dx.doi.org/10.1175/JCLI-D-11-00254.1.

Emanuel, K., 2007. Environmental factors affecting tropical Cyclone power dissipation. J. Clim. 20 (22), 5497–5509. http://dx.doi.org/10.1175/2007JCLI1571.1.

Emanuel, K., 2010. Tropical cyclone activity downscaled from NOAA-CIRES reanalysis, 1908–1958. J. Adv. Modelling Earth Syst. 2, 1. http://dx.doi.org/10.3894/JAMES.2010.2.1.

Enayati, M., Bozorg-Haddad, O., Bazrafshan, J., Hejabi, S., Chu, X., 2021. Bias correction capabilities of quantile mapping methods for rainfall and temperature variables. J. Water Clim. Chang. 12 (2), 401–419. http://dx.doi.org/10.2166/wcc.2020.261.

ETCCDI, 2022. Climate change indices. URL http://etccdi.pacificclimate.org/list_27_indices.shtml.

Feng, T., Tipton, Z., Xia, L., Chang, Y., 2019. Evaluation of CORDEX regional climate models in simulating extreme dry spells in southwest China. Front. Earth Sci. 7, http://dx.doi.org/10.3389/feart.2019.00294.

Gan, R., Li, D., Chen, C., Yang, F., Ma, X., 2022. Impacts of climate change on extreme precipitation in the upstream of Chushandian reservoir, China. Hydrol. Res. 53 (3), 504–518. http://dx.doi.org/10.2166/nh.2022.135.

Gasparrini, A., Guo, Y., Hashizume, M., Lavigne, E., Zanobetti, A., Schwartz, J., Tobias, A., Tong, S., Rocklöv, J., Forsberg, B., Leone, M., De Sario, M., Bell, M.L., Guo, Y.-L.L., Wu, C.-f., Kan, H., Yi, S.-M., de Sousa Zanotti Stagliorio Coelho, M., Saldiva, P.H.N., Honda, Y., Kim, H., Armstrong, B., 2015. Mortality risk attributable to high and low ambient temperature: a multicountry observational study. Lancet 386 (9991), 369–375. http://dx.doi.org/10.1016/S0140-6736(14)62114-0.

Giorgi, F., 2019. Thirty years of regional climate modeling: Where are we and where are we going next? J. Geophys. Res.: Atmos. http://dx.doi.org/10.1029/2018JD030094, 2018JD030094.

Giorgi, F., Coppola, E., Solmon, F., Mariotti, L., Sylla, M., Bi, X., Elguindi, N., Diro, G., Nair, V., Giuliani, G., Turuncoglu, U., Cozzini, S., Güttler, I., O'Brien, T., Tawfik, A., Shalaby, A., Zakey, A., Steiner, A., Stordal, F., Sloan, L., Brankovic, C., 2012. RegCM4: model description and preliminary tests over multiple CORDEX domains. Clim. Res. 52, 7–29. http://dx.doi.org/10.3354/cr01018.

Giorgi, F., Hewitson, B., Christensen, J., Hulme, M., Storch, H.V., Whetton, P., Jones, R., Mearns, L., Fu, C., 2001. Regional Climate Information, Eval- uation and Projections. Cambridge University Press, Cambridge, United Kingdom and New York, NY, USA.

Giorgi, F., Jones, C., Asrar, G.R., 2009. Addressing climate information needs at the regional level: the CORDEX framework. WMO Bull. 58 (3).

Gudmundsson, L., Bremnes, J.B., Haugen, J.E., Engen-Skaugen, T., 2012. Technical note: Downscaling RCM precipitation to the station scale using statistical transformations – A comparison of methods. Hydrol. Earth Syst. Sci. 16 (9), 3383–3390. http://dx.doi.org/10.5194/hess-16-3383-2012.

Guo, H., Xu, M., Hu, Q., 2011. Changes in near-surface wind speed in China: 1969–2005. Int. J. Climatol. 31 (3), 349–358. http://dx.doi.org/10.1002/joc.2091.

Gutiérrez, J.M., Maraun, D., Widmann, M., Huth, R., Hertig, E., Benestad, R., Roessler, O., Wibig, J., Wilcke, R., Kotlarski, S., San Martín, D., Herrera, S., Bedia, J., Casanueva, A., Manzanas, R., Iturbide, M., Vrac, M., Dubrovsky, M., Ribalaygua, J., Pórtoles, J., Räty, O., Räisänen, J., Hingray, B., Raynaud, D., Casado, M.J., Ramos, P., Zerenner, T., Turco, M., Bosshard, T., Štěpánek, P., Bartholy, J., Pongracz, R., Keller, D.E., Fischer, A.M., Cardoso, R.M., Soares, P.M.M., Czernecki, B., Pagé, C., 2019. An intercomparison of a large ensemble of statistical downscaling methods over Europe: Results from the VALUE perfect predictor cross-validation experiment. Int. J. Climatol. 39 (9), 3750–3785. http://dx.doi.org/10.1002/joc.5462.

Gutowski, W.J., Decker, S.G., Donavon, R.A., Pan, Z., Arritt, R.W., Takle, E.S., 2003. Temporal–spatial scales of observed and simulated precipitation in central U.S. climate. J. Clim. 16 (22), 3841–3847. http://dx.doi.org/10.1175/1520-0442(2003)016<3841:TSOOAS>2.0.CO;2.

Guzzetti, F., Peruccacci, S., Rossi, M., Stark, C.P., 2008. The rainfall intensity–duration control of shallow landslides and debris flows: an update. Landslides 5 (1), 3–17. http://dx.doi.org/10.1007/s10346-007-0112-1.

Haas, R., Pinto, J.G., Born, K., 2014. Can dynamically downscaled windstorm footprints be improved by observations through a probabilistic approach? J. Geophys. Res.: Atmos. 119 (2), 713–725. http://dx.doi.org/10.1002/2013JD020882.

Hanson, S., Nicholls, R., Ranger, N., Hallegatte, S., Corfee-Morlot, J., Herweijer, C., Chateau, J., 2011. A global ranking of port cities with high exposure to climate extremes. Clim. Change 104 (1), 89–111. http://dx.doi.org/10.1007/s10584-010-9977-4.

Harada, Y., Kamahori, H., Chiaki, K., Endo, H., Kobayashi, S., Ota, Y., Onoda, H., Onogi, K., Miyaoka, K., Takahashi, K., 2016. The JRA-55 reanalysis: Representation of atmospheric circulation and climate variability. J. Meteorol. Soc. Jpn. Ser. II 94 (3), 269–302. http://dx.doi.org/10.2151/jmsj.2016-015.

Heo, J.-H., Ahn, H., Shin, J.-Y., Kjeldsen, T.R., Jeong, C., 2019. Probability distributions for a quantile mapping technique for a bias correction of precipitation data: A case study to precipitation data under climate change. Water 11 (7), 1475. http://dx.doi.org/10.3390/w11071475.

Hersbach, H., Bell, B., Berrisford, P., Biavati, G., Horányi, A., Muñoz Sabater, J., Nicolas, J., Peubey, C., Radu, R., Rozum, I., Schepers, D., Simmons, A., Soci, C., Dee, D., Thépaut, J.N., 2018. ERA5 hourly data on single levels from 1979 to present. Copernicus climate change service (C3S) climate data store (CDS).

Hersbach, H., Bell, B., Berrisford, P., Hirahara, S., Horányi, A., Muñoz-Sabater, J., Nicolas, J., Peubey, C., Radu, R., Schepers, D., Simmons, A., Soci, C., Abdalla, S., Abellan, X., Balsamo, G., Bechtold, P., Biavati, G., Bidlot, J., Bonavita, M., De Chiara, G., Dahlgren, P., Dee, D., Diamantakis, M., Dragani, R., Flemming, J., Forbes, R., Fuentes, M., Geer, A., Haimberger, L., Healy, S., Hogan, R.J., Hólm, E., Janisková, M., Keeley, S., Laloyaux, P., Lopez, P., Lupu, C., Radnoti, G., de Rosnay, P., Rozum, I., Vamborg, F., Villaume, S., Thépaut, J.N., 2020. The ERA5 global reanalysis. Q. J. R. Meteorol. Soc. 146 (730), 1999–2049. http://dx.doi.org/10.1002/qj.3803.

Hersbach, H., Dee, D., 2016. ERA5 reanalysis is in production. ECMWF Newsl. 147, 7.

Hewitson, B., Crane, R., 1996. Climate downscaling: techniques and application. Clim. Res. 7, 85–95. http://dx.doi.org/10.3354/cr007085.

Huang, D.-Q., Zhu, J., Zhang, Y.-C., Huang, A.-N., 2013. Uncertainties on the simulated summer precipitation over eastern China from the CMIP5 models. J. Geophys. Res.: Atmos. 118 (16), 9035–9047. http://dx.doi.org/10.1002/jgrd.50695.

Ines, A.V., Hansen, J.W., 2006. Bias correction of daily GCM rainfall for crop simulation studies. Agricult. Forest Meteorol. 138 (1–4), 44–53. http://dx.doi.org/10.1016/j.agrformet.2006.03.009.

IPCC, 2013. Climate Change 2013: The Physical Science Basis. Contribution of Working Group I to the Fifth Assessment Report of the Intergovernmental Panel on Climate Change. Cambridge University Press, Cambridge, United Kingdom and New York, NY, USA, p. 1535. http://dx.doi.org/10.1017/CBO9781107415324.

IPCC, 2021. Climate Change 2021: The Physical Science Basis. Contribution of Working Group I to the Sixth Assessment Report of the Intergovernmental Panel on Climate Change. Cambridge University Press. In Press.

Iturbide, M., Bedia, J., Herrera, S., Baño-Medina, J., Fernández, J., Frías, M.D., Manzanas, R., San-Martín, D., Cimadevilla, E., Cofiño, A.S., Gutiérrez, J.M., 2018. The R-based climate4R open framework for reproducible climate data access and post-processing. Environ. Model. Softw. http://dx.doi.org/10.1016/j.envsoft.2018.09.009.

Iversen, T., Bentsen, M., Bethke, I., Debernard, J.B., Kirkevag, A., Seland, O., Drange, H., Kristjansson, J.E., Medhaug, I., Sand, M., Seierstad, I.A., 2013. The norwegian earth system model, NorESM1-M – part 2: Climate response and scenario projections. Geosci. Model Dev. 6 (2), 389–415. http://dx.doi.org/10.5194/gmd-6-389-2013.

Jacob, D., 2001. A note to the simulation of the annual and inter-annual variability of the water budget over the Baltic sea drainage basin. Meteorol. Atmos. Phys. 77 (1–4), 61–73. http://dx.doi.org/10.1007/s007030170017.

Jacob, D., Elizalde, A., Haensler, A., Hagemann, S., Kumar, P., Podzun, R., Rechid, D., Remedio, A.R., Saeed, F., Sieck, K., Teichmann, C., Wilhelm, C., 2012. Assessing the transferability of the regional climate model REMO to different coordinated regional climate downscaling experiment (CORDEX) regions. Atmosphere 3 (1), 181–199. http://dx.doi.org/10.3390/atmos3010181.

Jacobeit, J., Hertig, E., Seubert, S., Lutz, K., 2014. Statistical downscaling for climate change projections in the Mediterranean region: methods and results. Reg. Environ. Chang. 14 (5), 1891–1906. http://dx.doi.org/10.1007/s10113-014-0605-0.

Jin, C.S., Cha, D.H., Lee, D.K., Suh, M.S., Hong, S.Y., Kang, H.S., Ho, C.H., 2016. Evaluation of climatological tropical cyclone activity over the western north Pacific in the CORDEX-east Asia multi-RCM simulations. Clim. Dynam. 47 (3–4), 765–778. http://dx.doi.org/10.1007/s00382-015-2869-6.

Jolliff, J.K., Kindle, J.C., Shulman, I., Penta, B., Friedrichs, M.A., Helber, R., Arnone, R.A., 2009. Summary diagrams for coupled hydrodynamic-ecosystem model skill assessment. J. Mar. Syst. 76 (1–2), 64–82. http://dx.doi.org/10.1016/j.jmarsys.2008.05.014.

Jungclaus, J.H., Fischer, N., Haak, H., Lohmann, K., Marotzke, J., Matei, D., Mikolajewicz, U., Notz, D., Storch, J.S., 2013. Characteristics of the ocean simulations in the max Planck institute ocean model (MPIOM) the ocean component of the MPI-earth system model. J. Adv. Modelling Earth Syst. 5 (2), 422–446. http://dx.doi.org/10.1002/jame.20023.

Kalnay, E., Kanamitsu, M., Kistler, R., Collins, W., Deaven, D., Gandin, L., Iredell, M., Saha, S., White, G., Woollen, J., Zhu, Y., Chelliah, M., Ebisuzaki, W., Higgins, W., Janowiak, J., Mo, K.C., Ropelewski, C., Wang, J., Leetmaa, A., Reynolds, R., Jenne, R., Joseph, D., 1996. The NCEP/NCAR 40-year reanalysis project. Bull. Am. Meteorol. Soc. 77 (3), 437–472. http://dx.doi.org/10.1175/1520-0477(1996)077%3C0437:TNYRP%3E2.0.CO;2.

Kanamitsu, M., Ebisuzaki, W., Woollen, J., Yang, S.K., Hnilo, J.J., Fiorino, M., Potter, G.L., 2002. NCEP-DOE AMIP-II reanalysis (R-2). Bull. Am. Meteorol. Soc. 83 (11), 1631–1644. http://dx.doi.org/10.1175/BAMS-83-11.

Ke, Q., Tian, X., Bricker, J., Tian, Z., Guan, G., Cai, H., Huang, X., Yang, H., Liu, J., 2020. Urban pluvial flooding prediction by machine learning approaches – a case study of Shenzhen city, China. Adv. Water Resour. 145, 103719. http://dx.doi.org/10.1016/j.advwatres.2020.103719.

Ke, Q., Yin, J., Bricker, J.D., Savage, N., Buonomo, E., Ye, Q., Visser, P., Dong, G., Wang, S., Tian, Z., Sun, L., Toumi, R., Jonkman, S.N., 2021. An integrated framework of coastal flood modelling under the failures of sea dikes: a case study in Shanghai. Nat. Hazards 109 (1), 671–703. http://dx.doi.org/10.1007/s11069-021-04853-z.

Knutson, T., Camargo, S.J., Chan, J.C.L., Emanuel, K., Ho, C.-H., Kossin, J., Mohapatra, M., Satoh, M., Sugi, M., Walsh, K., Wu, L., 2020. Tropical Cyclones and climate change assessment: Part II: Projected response to anthropogenic warming. Bull. Am. Meteorol. Soc. 101 (3), E303–E322. http://dx.doi.org/10.1175/BAMS-D-18-0194.1.

Knutson, T.R., Sirutis, J.J., Zhao, M., Tuleya, R.E., Bender, M., Vecchi, G.A., Villarini, G., Chavas, D., 2015. Global projections of intense tropical Cyclone activity for the late twenty-first century from dynamical downscaling of CMIP5/RCP4.5 scenarios. J. Clim. 28 (18), 7203–7224. http://dx.doi.org/10.1175/JCLI-D-15-0129.1.

Kotlarski, S., Keuler, K., Christensen, O.B., Colette, A., Déqué, M., Gobiet, A., Goergen, K., Jacob, D., Lüthi, D., van Meijgaard, E., Nikulin, G., Schär, C., Teichmann, C., Vautard, R., Warrach-Sagi, K., Wulfmeyer, V., 2014. Regional climate modeling on European scales: a joint standard evaluation of the EURO-CORDEX RCM ensemble. Geosci. Model Dev. 7 (4), 1297–1333. http://dx.doi.org/10.5194/gmd-7-1297-2014.

Kouhestani, S., Eslamian, S.S., Abedi-Koupai, J., Besalatpour, A.A., 2016. Projection of climate change impacts on precipitation using soft-computing techniques: A case study in Zayandeh-rud Basin, Iran. Glob. Planet. Change 144, 158–170. http://dx.doi.org/10.1016/j.gloplacha.2016.07.013.

Lahoz, W.A., Schneider, P., 2014. Data assimilation: making sense of earth observation. Front. Environ. Sci. 2, http://dx.doi.org/10.3389/fenvs.2014.00016.

Lange, S., 2019. Trend-preserving bias adjustment and statistical downscaling with ISIMIP3basd (v1.0). Geosci. Model Dev. 12 (7), 3055–3070. http://dx.doi.org/10.5194/gmd-12-3055-2019.

Latombe, G., Burke, A., Vrac, M., Levavasseur, G., Dumas, C., Kageyama, M., Ramstein, G., 2018. Comparison of spatial downscaling methods of general circulation model results to study climate variability during the last Glacial maximum. Geosci. Model Dev. 11 (7), 2563–2579. http://dx.doi.org/10.5194/gmd-11-2563-2018.

Laux, P., Rötter, R.P., Webber, H., Dieng, D., Rahimi, J., Wei, J., Faye, B., Srivastava, A.K., Bliefernicht, J., Adeyeri, O., Arnault, J., Kunstmann, H., 2021. To bias correct or not to bias correct? An agricultural impact modelers' perspective on regional climate model data. Agricult. Forest Meteorol. 304–305, 108406. http://dx.doi.org/10.1016/j.agrformet.2021.108406, URL https://www.sciencedirect.com/science/article/pii/S0168192321000897.

Li, Y., Bai, J., You, Z., Hou, J., Li, W., 2021. Future changes in the intensity and frequency of precipitation extremes over China in a warmer world: Insight from a large ensemble. PLOS ONE 16 (5), e0252133. http://dx.doi.org/10.1371/journal.pone.0252133.

Li, D., Feng, J., Xu, Z., Yin, B., Shi, H., Qi, J., 2019. Statistical bias correction for simulated wind speeds over CORDEX-east Asia. Earth Space Sci. 6 (2), 200–211. http://dx.doi.org/10.1029/2018EA000493.

Li, H., Sheffield, J., Wood, E.F., 2010. Bias correction of monthly precipitation and temperature fields from intergovernmental panel on climate change AR4 models using equidistant quantile matching. J. Geophys. Res. 115 (D10), D10101. http://dx.doi.org/10.1029/2009JD012882.

Lu, R.-Y., Chen, R.-D., 2016. A review of recent studies on extreme heat in China. Atmospheric Ocean. Sci. Lett. 9 (2), 114–121. http://dx.doi.org/10.1080/16742834.2016.1133071.

Ma, W., Chen, R., Kan, H., 2014. Temperature-related mortality in 17 large Chinese cities: How heat and cold affect mortality in China. Environ. Res. 134, 127–133. http://dx.doi.org/10.1016/j.envres.2014.07.007.

Mann, H.B., Whitney, D.R., 1947. On a test of whether one of two random variables is stochastically larger than the other. Ann. Math. Stat. 18 (1), 50–60. http://dx.doi.org/10.1214/aoms/1177730491.

Maraun, D., 2012. Nonstationarities of regional climate model biases in European seasonal mean temperature and precipitation sums. Geophys. Res. Lett. 39 (6), n/a–n/a. http://dx.doi.org/10.1029/2012GL051210.

Maraun, D., 2013. Bias correction, quantile mapping, and downscaling: Revisiting the inflation issue. J. Clim. 26 (6), 2137–2143. http://dx.doi.org/10.1175/JCLI-D-12-00821.1.

Maraun, D., 2016. Bias correcting climate change simulations - a critical review. Curr. Clim. Chang. Rep. 2 (4), 211–220. http://dx.doi.org/10.1007/s40641-016-0050-x.

Maraun, D., Wetterhall, F., Ireson, A.M., Chandler, R.E., Kendon, E.J., Widmann, M., Brienen, S., Rust, H.W., Sauter, T., Themeßl, M., Venema, V.K.C., Chun, K.P., Goodess, C.M., Jones, R.G., Onof, C., Vrac, M., Thiele-Eich, I., 2010. Precipitation downscaling under climate change: Recent developments to bridge the gap between dynamical models and the end user. Rev. Geophys. 48 (3), RG3003. http://dx.doi.org/10.1029/2009RG000314.

Martius, O., Pfahl, S., Chevalier, C., 2016. A global quantification of compound precipitation and wind extremes. Geophys. Res. Lett. 43 (14), 7709–7717. http://dx.doi.org/10.1002/2016GL070017.

Martynov, A., Laprise, R., Sushama, L., Winger, K., Šeparović, L., Dugas, B., 2013. Reanalysis-driven climate simulation over CORDEX north America domain using the Canadian regional climate model, version 5: model performance evaluation. Clim. Dynam. 41 (11–12), 2973–3005. http://dx.doi.org/10.1007/s00382-013-1778-9.

Maurer, E.P., Hidalgo, H.G., 2008. Utility of daily vs. monthly large-scale climate data: an intercomparison of two statistical downscaling methods. Hydrol. Earth Syst. Sci. 12 (2), 551–563. http://dx.doi.org/10.5194/hess-12-551-2008.

Maurer, E.P., Pierce, D.W., 2014. Bias correction can modify climate model simulated precipitation changes without adverse effect on the ensemble mean. Hydrol. Earth Syst. Sci. 18 (3), 915–925. http://dx.doi.org/10.5194/hess-18-915-2014.

Messmer, M., Simmonds, I., 2021. Global analysis of cyclone-induced compound precipitation and wind extreme events. Weather Clim. Extrem. 32, 100324. http://dx.doi.org/10.1016/j.wace.2021.100324.

Miao, C., Su, L., Sun, Q., Duan, Q., 2016. A nonstationary bias-correction technique to remove bias in GCM simulations. J. Geophys. Res.: Atmos. 121 (10), 5718–5735. http://dx.doi.org/10.1002/2015JD024159.

Pastén-Zapata, E., Jones, J.M., Moggridge, H., Widmann, M., 2020. Evaluation of the performance of euro-CORDEX regional climate models for assessing hydrological climate change impacts in great Britain: A comparison of different spatial resolutions and quantile mapping bias correction methods. J. Hydrol. 584, http://dx.doi.org/10.1016/j.jhydrol.2020.124653.

Piani, C., Haerter, J.O., Coppola, E., 2010a. Statistical bias correction for daily precipitation in regional climate models over Europe. Theor. Appl. Climatol. 99 (1–2), 187–192. http://dx.doi.org/10.1007/s00704-009-0134-9.

Piani, C., Weedon, G., Best, M., Gomes, S., Viterbo, P., Hagemann, S., Haerter, J., 2010b. Statistical bias correction of global simulated daily precipitation and temperature for the application of hydrological models. J. Hydrol. 395 (3–4), 199–215. http://dx.doi.org/10.1016/j.jhydrol.2010.10.024.

R. Core Team, 2017. R: A language and environment for statistical computing. URL https://www.R-project.org/.

Reifen, C., Toumi, R., 2009. Climate projections: Past performance no guarantee of future skill? Geophys. Res. Lett. 36 (13), L13704. http://dx.doi.org/10.1029/2009GL038082.

Ridder, N.N., Pitman, A.J., Westra, S., Ukkola, A., Do, H.X., Bador, M., Hirsch, A.L., Evans, J.P., Di Luca, A., Zscheischler, J., 2020. Global hotspots for the occurrence of compound events. Nature Commun. 11 (1), 5956. http://dx.doi.org/10.1038/s41467-020-19639-3.

Sarica, G.M., Zhu, T., Jian, W., Lo, E.Y.-M., Pan, T.-C., 2021. Spatio-temporal dynamics of flood exposure in shenzhen from present to future. Environ. Plan. B: Urban Anal. City Sci. 48 (5), 1011–1024. http://dx.doi.org/10.1177/2399808321991540.

Shen, C., Duan, Q., Miao, C., Xing, C., Fan, X., Wu, Y., Han, J., 2020. Bias correction and ensemble projections of temperature changes over ten subregions in CORDEX east Asia. Adv. Atmospheric Sci. 37 (11), 1191–1210. http://dx.doi.org/10.1007/s00376-020-0026-6.

Shin, J.-Y., Lee, T., Park, T., Kim, S., 2019. Bias correction of RCM outputs using mixture distributions under multiple extreme weather influences. Theor. Appl. Climatol. 137 (1–2), 201–216. http://dx.doi.org/10.1007/s00704-018-2585-3.

Shinya, K., Ota, Y., Harada, Y., Ebita, A., Moriya, M., Onoda, H., Onogi, K., Kamahori, H., Kobayashi, C., Endo, H., Miyaoka, K., Takahashi, K., 2015. The JRA-55 reanalysis: General specifications and basic characteristics. J. Meteorol. Soc. Jpn. Ser. II 93 (1), 5–48. http://dx.doi.org/10.2151/jmsj.2015-001.

Stevens, B., Giorgetta, M., Esch, M., Mauritsen, T., Crueger, T., Rast, S., Salzmann, M., Schmidt, H., Bader, J., Block, K., Brokopf, R., Fast, I., Kinne, S., Kornblueh, L., Lohmann, U., Pincus, R., Reichler, T., Roeckner, E., 2013. Atmospheric component of the MPI-M earth system model: ECHAM6. J. Adv. Modelling Earth Syst. 5 (2), 146–172. http://dx.doi.org/10.1002/jame.20015.

Student, 1908. The probable error of a mean. Biometrika 1–25.

Sun, J., Ao, J., 2013. Changes in precipitation and extreme precipitation in a warming environment in China. Chin. Sci. Bull. 58 (12), 1395–1401. http://dx.doi.org/10.1007/s11434-012-5542-z.

Tang, J., Xiao, Y., Hui, P., Lu, Y., Yu, K., 2022. Reanalysis-driven multi-RCM high-resolution simulation of precipitation within CORDEX east Asia phase II. Int. J. Climatol. http://dx.doi.org/10.1002/joc.7592.

Taylor, K.E., 2001. Summarizing multiple aspects of model performance in a single diagram. J. Geophys. Res.: Atmos. 106 (D7), 7183–7192. http://dx.doi.org/10.1029/2000JD900719.

Teutschbein, C., Seibert, J., 2012. Bias correction of regional climate model simulations for hydrological climate-change impact studies: Review and evaluation of different methods. J. Hydrol. 456–457, 12–29. http://dx.doi.org/10.1016/j.jhydrol.2012.05.052.

Themeßl, M.J., Gobiet, A., Heinrich, G., 2012. Empirical-statistical downscaling and error correction of regional climate models and its impact on the climate change signal. Clim. Change 112 (2), 449–468. http://dx.doi.org/10.1007/s10584-011-0224-4.

Tong, Y., Gao, X., Han, Z., Xu, Y., Xu, Y., Giorgi, F., 2021. Bias correction of temperature and precipitation over China for RCM simulations using the QM and QDM methods. Clim. Dynam. 57 (5–6), 1425–1443. http://dx.doi.org/10.1007/s00382-020-05447-4.

Torres-Alavez, J.A., Glazer, R., Giorgi, F., Coppola, E., Gao, X., Hodges, K.I., Das, S., Ashfaq, M., Reale, M., Sines, T., 2021. Future projections in tropical cyclone activity over multiple CORDEX domains from RegCM4 CORDEX-CORE simulations. Clim. Dynam. 57 (5–6), 1507–1531. http://dx.doi.org/10.1007/s00382-021-05728-6.

Truchelut, R.E., Hart, R.E., 2011. Quantifying the possible existence of undocumented Atlantic warm-core cyclones in NOAA/CIRES 20th century reanalysis data. Geophys. Res. Lett. 38 (8), n/a–n/a. http://dx.doi.org/10.1029/2011GL046756.

Truchelut, R.E., Hart, R.E., Luthman, B., 2013. Global identification of previously undetected pre-satellite-era tropical Cyclone candidates in NOAA/CIRES twentieth-century reanalysis data. J. Appl. Meteorol. Climatol. 52 (10), 2243–2259. http://dx.doi.org/10.1175/JAMC-D-12-0276.1.

Van Den Besselaar, E., Van Der Schrier, G., Cornes, R.C., Klein Tank, A.M.G., 2017. SA-OBS: A daily gridded surface temperature and precipitation dataset for southeast Asia. J. Clim. 30 (14), 5151–5165. http://dx.doi.org/10.1175/JCLI-D-16-0575.s1.

Vecchi, G.A., Soden, B.J., 2007. Increased tropical Atlantic wind shear in model projections of global warming. Geophys. Res. Lett. 34 (8), http://dx.doi.org/10.1029/2006GL028905.

Walsh, K., 1997. Objective detection of tropical Cyclones in high-resolution analyses. Mon. Weather Rev. 125 (8), 1767–1779. http://dx.doi.org/10.1175/1520-0493(1997)125<1767:ODOTCI>2.0.CO;2.

Walsh, K.J.E., Fiorino, M., Landsea, C.W., McInnes, K.L., 2007. Objectively determined resolution-dependent threshold criteria for the detection of tropical Cyclones in climate models and reanalyses. J. Clim. 20 (10), 2307–2314. http://dx.doi.org/10.1175/JCLI4074.1.

Wilby, R.L., Harris, I., 2006. A framework for assessing uncertainties in climate change impacts: Low-flow scenarios for the river Thames, UK. Water Resour. Res. 42 (2), http://dx.doi.org/10.1029/2005WR004065.

Wilcoxon, F., 1945. Individual comparisons by ranking methods. Biom. Bull. 1 (6), 80. http://dx.doi.org/10.2307/3001968.

Wong, J.S., Razavi, S., Bonsal, B.R., Wheater, H.S., Asong, Z.E., 2017. Inter-comparison of daily precipitation products for large-scale hydro-climatic applications over Canada. Hydrol. Earth Syst. Sci. 21 (4), 2163–2185. http://dx.doi.org/10.5194/hess-21-2163-2017.

Wu, J., Zha, J., Zhao, D., 2016. Estimating the impact of the changes in land use and cover on the surface wind speed over the east China plain during the period 1980–2011. Clim. Dynam. 46 (3–4), 847–863. http://dx.doi.org/10.1007/s00382-015-2616-z.

Wu, J., Zha, J., Zhao, D., Yang, Q., 2018. Changes in terrestrial near-surface wind speed and their possible causes: an overview. Clim. Dynam. 51 (5–6), 2039–2078. http://dx.doi.org/10.1007/s00382-017-3997-y.

Xu, Y., 2020. Hyfo: Hydrology and climate forecasting. URL https://CRAN.R-project.org/package=hyfo.

Xu, W., Lei, X., Chen, S., Yu, T., Hu, Z., Zhang, M., Jiang, L., Bao, R., Guan, X., Ma, M., Wei, J., Gao, L., Feng, A., 2022a. How well does the ERA5 reanalysis capture the extreme climate events over China? Part II: Extreme temperature. Front. Environ. Sci. 10, http://dx.doi.org/10.3389/fenvs.2022.921659.

Xu, H., Tian, Z., Sun, L., Ye, Q., Ragno, E., Bricker, J., Mao, G., Tan, J., Wang, J., Ke, Q., Wang, S., Toumi, R., 2022b. Compound flood impact of water level and rainfall during tropical cyclone period in a coastal city: The case of Shanghai. Nat. Hazards Earth Syst. Sci. Discuss. 2022, 1–19. http://dx.doi.org/10.5194/nhess-2022-26.

Zhang, X., Alexander, L., Hegerl, G.C., Jones, P., Tank, A.K., Peterson, T.C., Trewin, B., Zwiers, F.W., 2011. Indices for monitoring changes in extremes based on daily temperature and precipitation data. WIREs Clim. Chang. 2 (6), 851–870. http://dx.doi.org/10.1002/wcc.147.

Zhang, Y., Sun, X., Chen, C., 2021. Characteristics of concurrent precipitation and wind speed extremes in China. Weather Clim. Extrem. 32, 100322. http://dx.doi.org/10.1016/j.wace.2021.100322.

Zhang, Y., Yu, C., Bao, J., Li, X., 2017. Impact of temperature on mortality in Hubei, China: a multi-county time series analysis. Sci. Rep. 7 (1), 45093. http://dx.doi.org/10.1038/srep45093.

Zhang, W., Zhou, T., 2020. Increasing impacts from extreme precipitation on population over China with global warming. Sci. Bull. 65 (3), 243–252. http://dx.doi.org/10.1016/j.scib.2019.12.002.

Zscheischler, J., Martius, O., Westra, S., Bevacqua, E., Raymond, C., Horton, R.M., van den Hurk, B., AghaKouchak, A., Jézéquel, A., Mahecha, M.D., Maraun, D., Ramos, A.M., Ridder, N.N., Thiery, W., Vignotto, E., 2020. A typology of compound weather and climate events. Nat. Rev. Earth Environ. 1 (7), 333–347. http://dx.doi.org/10.1038/s43017-020-0060-z.

Zscheischler, J., Naveau, P., Martius, O., Engelke, S., C. Raible, C., 2021. Evaluating the dependence structure of compound precipitation and wind speed extremes. Earth Syst. Dyn. 12 (1), 1–16. http://dx.doi.org/10.5194/esd-12-1-2021.

Zscheischler, J., Westra, S., Van Den Hurk, B.J., Seneviratne, S.I., Ward, P.J., Pitman, A., Aghakouchak, A., Bresch, D.N., Leonard, M., Wahl, T., Zhang, X., 2018. Future climate risk from compound events. Nat. Clim. Chang. 8 (6), 469–477. http://dx.doi.org/10.1038/s41558-018-0156-3.